Geochemistry Geophysics Geosystems G3
AN ELECTRONIC JOURNAL OF THE EARTH SCIENCES
Published by AGU and the Geochemical Society

Article
Volume 10
8 May 2009
Q0AB01, doi:10.1029/2008GC002293
ISSN: 1525-2027

Low lower crustal velocity across Ethiopia: Is the Main Ethiopian Rift a narrow rift in a hot craton?

Katie M. Keranen
Department of Geophysics, Stanford University, 397 Panama Mall, Stanford, California 94305, USA

Now at U.S. Geological Survey, Seattle, Washington 98195, USA (kkeranen@usgs.gov)

Simon L. Klemperer
Department of Geophysics, Stanford University, 397 Panama Mall, Stanford, California 94305, USA

Jordi Julia
Department of Geosciences, Pennsylvania State University, 503 Deike Building, University Park, Pennsylvania 16802, USA

Jesse F. Lawrence
Department of Geophysics, Stanford University, 397 Panama Mall, Stanford, California 94305, USA

Andy A. Nyblade
Department of Geosciences, Pennsylvania State University, 503 Deike Building, University Park, Pennsylvania 16802, USA

[1] The Main Ethiopian Rift (MER) is a classic narrow rift that developed in hot, weak lithosphere, not in the initially cold, thick, and strong lithosphere that would be predicted by common models of rift mode formation. Our new 1-D seismic velocity profiles from Rayleigh wave/receiver function joint inversion across the MER and the Ethiopian Plateau indicate that hot lower crust and upper mantle are present throughout the broad region affected by Oligocene flood basalt volcanism, including both the present rift and the adjacent Ethiopian Plateau hundreds of kilometers from the rift valley. The region of hot lithosphere closely corresponds to the region of flood basalt volcanism, and we interpret that the volcanism and thermal perturbation were jointly caused by impingement of the Afar plume head. Across the affected region, Vs is 3.6–3.8 km/s in the lowermost crust and $\leq$4.3 km/s in the uppermost mantle, both $\sim$0.3 km/s lower than in the eastern and western branches of the East African Rift System to the south. We interpret the low Vs in the lower crust and upper mantle as indicative of hot lithosphere with partial melt. Our results lead to a hybrid rift mode, in which the brittle upper crust has developed as a narrow rift along the Neoproterozoic suture between East and West Gondwana, while at depth lithospheric deformation is distributed over the broad region ($\sim$400 km wide) thermally perturbed by the broad thermal upwelling associated with the Afar plume head. Development of both the East African Rift System to the south (in cold, strong lithosphere) and the MER to the north (in hot, weak lithosphere) as narrow rifts, despite their vastly different initial thermal states and depth-integrated lithospheric strength, indicates that common models of rift mode formation that focus only on temperature, thickness, and vertical strength profiles do not apply to these classic continental rifts. Instead, inherited structure and associated lithospheric weaknesses are the primary control on the mode of extension.

Components: 13,638 words, 18 figures, 2 tables.

Keywords: Ethiopia; continental extension; continental lithosphere; receiver functions; surface-wave inversion.

Index Terms: 7255 Seismology: Surface waves and free oscillations; 7218 Seismology: Lithosphere (1236); 7205 Seismology: Continental crust (1219); 8109 Tectonophysics: Continental tectonics: extensional (0905).

Received 22 October 2008; **Revised** 4 March 2009; **Accepted** 16 March 2009; **Published** 8 May 2009.

Keranen, K. M., S. L. Klemperer, J. Julia, J. F. Lawrence, and A. A. Nyblade (2009), Low lower crustal velocity across Ethiopia: Is the Main Ethiopian Rift a narrow rift in a hot craton?, *Geochem. Geophys. Geosyst.*, *10*, Q0AB01, doi:10.1029/2008GC002293.

Theme: Magma-Rich Extensional Regimes
Guest Editors: R. Meyer, J. van Wijk, A. Breivik, and C. Tegner

1. Introduction and Motivation

[2] There is an ongoing debate about the strength of crust and lithosphere in regions of extension. Knowledge of the rheological stratification of the lithosphere in these areas is a critical parameter in developing useful and accurate models of continental extension. Both simple analytical models, e.g., the commonly cited model of *Buck* [1991], and numerous thermomechanical geodynamic models of large-scale lithospheric extension [e.g., *Corti*, 2004; *van Wijk*, 2005; *Dyksterhuis et al.*, 2007; *Sokoutis et al.*, 2007; *Corti*, 2008] depend upon the assignment of accurate rheologic parameters in the crust and upper mantle. The thermal structure of the lithosphere, rheological stratification, and crustal thickness are required for this modeling, yet detailed and three-dimensional information of this type is not commonly available. Adding further complication is the understanding that the rheological stratification may change at different stages in rifting, as has been suggested for the Iberia–Newfoundland and Alpine Tethys margins [*Manatschal et al.*, 2007] and for the Main Ethiopian Rift [*Keranen and Klemperer*, 2008]. Broadly distributed data from the 2001–2003 EAGLE (Ethiopia-Afar Geoscientific Lithospheric Experiment [*Maguire et al.*, 2003]) and the 2000–2002 EBSE (Ethiopian Broadband Seismic Experiment [*Nyblade and Langston*, 2002]) seismic experiments in Ethiopia provide an opportunity in the MER, a classic example of a "narrow continental rift," to obtain a three-dimensional snapshot of crustal and upper mantle rheology immediately prior to breakup. We use shear wave seismic velocity profiles from our new joint inversion of surface wave dispersion curves and receiver functions using the methodology of *Julia et al.* [2000] to infer lithospheric rheology over a region including the MER and the adjacent Ethiopian and Somali Plateaus. *Dugda et al.* [2007] also used this joint inversion method in Ethiopia and Djibouti to study shear wave velocity structure using data from the EBSE array. Their study focused on the upper mantle and revealed thin lithosphere and low shear wave velocity in the uppermost mantle beneath the MER and the Ethiopian Plateau. Our study builds on *Dugda et al.* [2007] by providing detailed crustal velocity profiles beneath both the EBSE and EAGLE Phase I broadband stations, and by studying spatial variations in the crustal and upper mantle velocity structure with respect to the domains previously recognized by *Keranen and Klemperer* [2008]. We use our joint inversion results to infer the spatially variant rheology of the MER and adjacent plateaus and on the basis of this rheologic structure we propose a hybrid mode of continental extension. We additionally provide modelers with constraints on rheology of the crust and upper mantle in a classic narrow rift.

2. Tectonic Background

[3] The MER is a seismically and volcanically active portion of the East African Rift System (EARS) trending NE across the Ethiopian plateau (Figure 1). The MER developed within the Mozambique Belt, a broad Neoproterozoic mobile belt that extends from Ethiopia south through Kenya, Tanzania and Mozambique. The Mozambique Belt is believed to represent a Himalayan-type continental collision zone [*Burke and Sengor*,

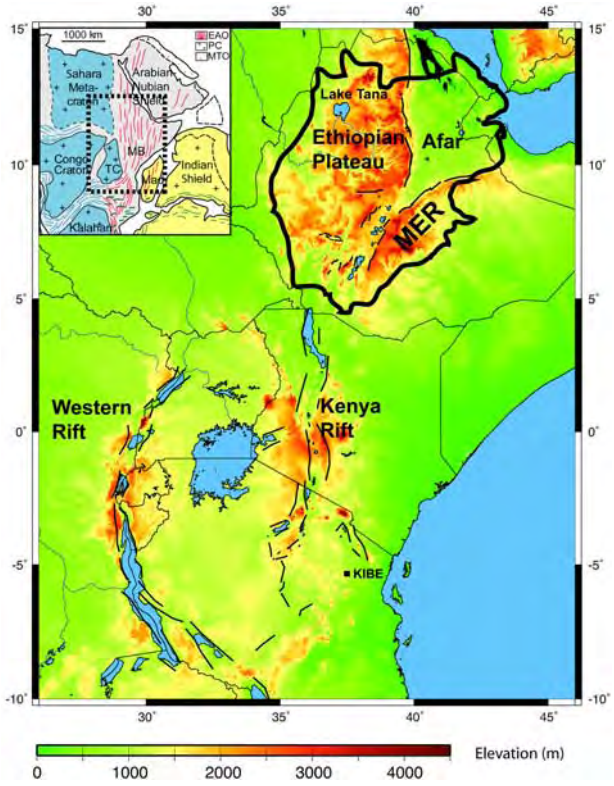

Figure 1. Map of East African Rift System. The heavy black line outlines the Ethiopian flood basalt province [from *Mohr*, 1983]. Lake Tana is the site of off-rift Quaternary volcanism and Oligocene and Quaternary xenoliths [*Conticelli et al.*, 1999]. The inset map shows the outline of Figure 1 (heavy dashed box) with respect to the cratons/shields and orogens forming East (yellow) and West (blue) Gondwana (modified from *Meert and Lieberman* [2008]). EAO, East African Orogen; MTO, Mesozoic-Tertiary Orogen; PC, Precambrian Shield; MB: Mozambique Belt; TC, Tanzanian Craton.

1986; *Shackleton*, 1986; *Stern*, 1994], and ophiolites mark numerous sutures within the basement complex of Ethiopia [*Vail*, 1985; *Berhe*, 1990; *Stern et al.*, 1990] although the trend of the sutures is contentious [*Church*, 1991]. The suture is also evident in neodymium (Nd) isotopic data [*Stern*, 2002], which indicates a major crustal boundary in Ethiopia separating juvenile crust in the north and west (mean age 0.87 Ga) from reworked Paleoproterozoic and Archean crust (mean age 2.0 Ga) to the east [*Stern*, 2002].

[4] Because of the continuity of the Mozambique Belt (Figure 1), the MER is commonly thought to have developed in lithosphere with a rheological structure much like that adjacent to the EARS further south where, away from the Cenozoic rift, the lithosphere is cold, thick, and strong on the basis of high seismic velocities [*Mechie et al.*, 1997], low heat flow [*Nyblade et al.*, 1990], and deep crustal earthquakes [*Foster et al.*, 1997]. The MER is unique, however, in that the heterogeneous Precambrian craton has been significantly modified by Tertiary plume magmatism. Flood basalts erupted primarily between 31 and 29 Ma cover much of the Proterozoic basement beneath the Ethiopian Plateau (Figure 1), extending over an area ~1000 km in diameter and reaching up to 2 km in thickness [*Baker et al.*, 1996; *Hofmann et al.*, 1997; *Ukstins et al.*, 2002]. In contrast to these Ethiopian flood basalts, which were erupted over a short time period ~20 ma prior to the onset of extension and cover the broad region of topographic doming, magmatism in the Kenya Rift to the south has occurred in stages roughly coeval with extension and is located in or near the rift valley rather than over the Kenya dome [*Macdonald*, 2002]. A mantle slow velocity anomaly associated with the Afar plume underlies the MER and the NW plateau [*Bastow et al.*, 2005; *Benoit et al.*, 2006a; *Bastow et al.*, 2008] down to at least 650 km depth beneath Afar and rising to at least 75 km depth beneath the Main Ethiopian Rift and NW Ethiopian Plateau.

[5] Since the eruption of the flood basalts in Ethiopia at 31–29 Ma, volcanism has continued both in the rift and on the adjacent plateaus. Two periods of volcanism at 22 Ma and from 10 to 7 Ma created a series of shield volcanoes on the northwest Ethiopian Plateau [*Kieffer et al.*, 2004]. A period of volcanism from 10 to 12 Ma occurred within the MER, and bimodal Quaternary volcanism occurred both within the MER and on the northwest Ethiopian Plateau near Lake Tana, hundreds of kilometers from the rift valley [*Abate et al.*, 1998; *Conticelli et al.*, 1999].

[6] Lithospheric structures that developed within Ethiopia prior to the onset of Cenozoic rifting have controlled the evolution of the Main Ethiopian Rift, which is interpreted to have propagated in an irregular temporal and spatial manner [*Bonini et al.*, 2005; *Keranen and Klemperer*, 2008]. The irregular propagation has created discontinuities along the strike of the rift, separating the northern (NMER), central (CMER) and southern (SMER) sectors (Figure 2). On the western shoulder two distinct domains are also interpreted, the NW and SW shoulders, on the basis of a sharp change in

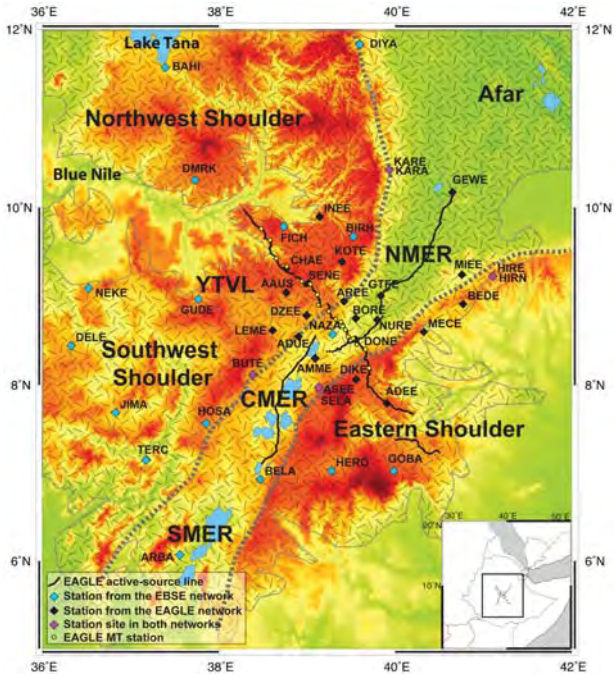

Figure 2. Map of the Main Ethiopian Rift showing broadband stations (diamonds), EAGLE active source profiles (continuous black lines), the EAGLE MT stations (yellow circles), and the distribution of flood basalts (cross hatching) [from *Mohr*, 1983]. Indentations into the flood basalt distribution in this region are largely erosional (e.g., the gorge of the Blue Nile), but flood basalts pinch out to the SE. The dashed gray lines outline the structural rift valley. Stations used in our joint inversion are labeled; stations with two names were colocated in the EAGLE and EBSE networks. YTVL, Yerer-Tullu Wellel Volcano-tectonic Lineament, an ~E-W trending zone separating the NW and SW shoulders [*Keranen and Klemperer*, 2008]. The inset map shows the location of the active source profiles in the Horn of Africa.

crustal thickness between the two domains from ~40 km to ~35 km respectively (Figure 2).

3. Method

[7] We use the method of *Julia et al.* [2000] for our joint inversion of two independent data sets: receiver function waveforms and Rayleigh wave group velocities. Jointly inverting these two data sets is now a standard technique in seismic investigations of the lithosphere. Although receiver function inversions provide detailed profiles of lithospheric discontinuity structure, they offer only weak constraints on the absolute velocity in each layer. Inversions of surface wave dispersion curves provide a smooth profile of the absolute velocity structure. Combining the two data sets in a joint inversion therefore provides a well-constrained profile of the lithospheric velocity and discontinuity structure. The inversion method of *Julia et al.* [2000] has been used in numerous investigations [e.g., *Julia et al.*, 2003; *Horspool et al.*, 2006; *Dugda et al.*, 2007; *Gok et al.*, 2008], and other methods developed to jointly invert these two data types are also commonly employed [e.g., *Lawrence and Wiens*, 2004; *Chang and Baag*, 2005; *Tkalcic et al.*, 2006]. Details on consistency and complementarity of the two data sets, as well as weighting and normalization of input data, are available in the original methodological paper of *Julia et al.* [2000]. While readers are urged to consult that paper for the complete methodology, we summarize the method and our slight modifications below.

[8] The method [*Julia et al.*, 2000] that we employ makes use of a linearized inversion procedure that minimizes a weighted combination of least squares norms for each data set. These norms are a model roughness norm and a vector difference norm between inverted and preset model parameters. The velocity models obtained are, consequently, a compromise between fitting each of the observations, model simplicity and a priori constraints. To make the contribution of each data set to the joint least squares misfit comparable, a normalization of the data set is necessary, and this is done using the number of data points and variance for each of the data sets. An influence factor is then used to control the trade-off between fitting the receiver functions and the group velocity curves [*Julia et al.*, 2000].

3.1. Data

[9] Seismic data used in this study are from two networks. Data were collected from 2001 to 2003 by the EAGLE Phase I network [*Stuart et al.*, 2006] and from 2000 to 2002 by the Ethiopia broadband seismic experiment (EBSE) [*Nyblade and Langston*, 2002]. The 30 stations of the EAGLE Phase I network were located primarily within the MER (Figure 2), with several stations on the nearby shoulders. Twenty-two of the 27 seismic stations in the EBSE were located either on the eastern or western side of the Ethiopian Plateau (Figure 2) with the rest of the stations in the MER or Afar Depression. In our joint inversion, we use our own computed receiver functions from 39 of the available stations and previously published fundamental mode Rayleigh wave group velocities [*Pasyanos*, 2005]. The remaining stations were

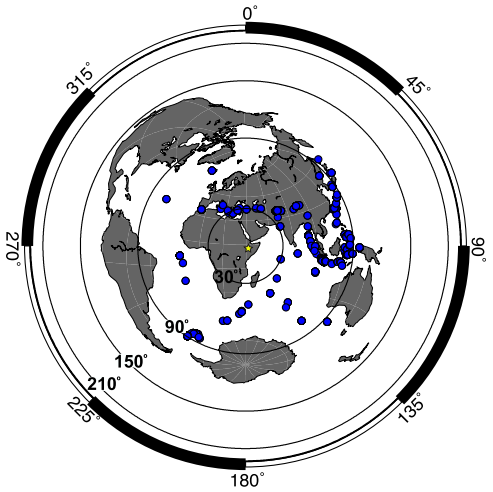

Figure 3. Distribution of earthquakes used for receiver function analysis. 148 earthquakes with Mw > 5.5 at offsets of 30° to 95° were used. The yellow star represents the location of the center of our study.

either outside of our area of interest or had unreliable data quality (most as a result of equipment malfunction). Love wave group velocities were not included because there are few high-quality measurements available for Ethiopia [*Benoit*, 2005].

3.2. Rayleigh Wave Group Velocities

[10] Rayleigh wave group velocities of 15 to 75 s period from the model of *Pasyanos* [2005] were used for the joint inversion. The model of Pasyanos includes group velocity measurements from *Benoit et al.* [2006b], who added new measurements made with data from the EBSE to the dispersion measurements of *Pasyanos et al.* [2001] for a surface wave tomography study of eastern Africa. Typical uncertainties in group velocities range between 0.01 and 0.02 km/s but increase to 0.02 and 0.03 km/s for the shortest periods in the Pasyanos model. It is far better to use inverted group velocities, as we do in our joint inversion, than raw dispersion measurements because the inverted values represent laterally localized structure. *Pasyanos* [2005] suggests the resolution of his model may be as low as 1° for periods less than 30 s, and 2° for longer periods. Velocity functions are extracted from his model at each station used in our inversion.

3.3. Receiver Functions

[11] Receiver functions were computed at 39 stations using 2462 seismograms from 148 teleseismic events between distances of 30° and 95° with magnitudes greater than 5.5 Mw. Most of the events are from the east (the Indonesian and Western Pacific subduction zones) or the northeast (Hindu Kush-Pamir region) (Figure 3). The maximum number of events stacked together to form a single receiver function was 46.

[12] We used the time domain iterative deconvolution method of *Ligorria and Ammon* [1999] to compute the receiver functions, and we evaluated the quality of the receiver functions using a least squares misfit criterion. This misfit criterion provides a measure of the closeness of a receiver function to an ideal case, and is calculated by using the difference between the radial component seismogram and the convolution of the vertical component seismogram with the predicted radial receiver function. Receiver functions with a fit of 90% and above were used in the inversion. The receiver functions were filtered with a Gaussian low-pass filter using three distinct filter width parameters of 0.5, 1.0 and 2.5 (pulse widths of approximately 2.36, 1.67, and 1.0 s) to obtain low-, middle-, and high-frequency receiver functions, respectively. Radial and tangential receiver functions were visually examined for evidence of lateral heterogeneity and for dipping structure. Events with large-amplitude tangential receiver functions were not used.

[13] In the joint inversion, we used four groups of receiver functions each corresponding to a range of ray parameters from 0.04 to 0.049 s/km, from 0.05 to 0.059 s/km, from 0.060 to 0.069 s/km, and from 0.070 to 0.079 s/km. For each grouping of receiver functions, we computed and stacked the three sets of receiver functions with overlapping frequency bands described previously. The range of frequencies was chosen to be able to distinguish between gradational and sharp boundaries in lithospheric structure [*Julia*, 2007].

[14] For the receiver functions the lateral distance from the station sampled by the Ps phase at the Moho is 4 km and 7 km for crustal thicknesses of 25 km and 45 km for a ray parameter of 0.04 s/km, and 7 km and 13 km for a ray parameter of 0.079 s/km, so that the spatial resolution is significantly better than for the surface wave model.

3.4. Initial Models

[15] The initial models used for the inversion consisted of constant velocity layers that increase in thickness with depth. Layer thicknesses were 0.5 km for the top 1.5 km, 1 km to 5.5 km, 2.5 km between 5.5 and 53 km depth, 5 km between 53

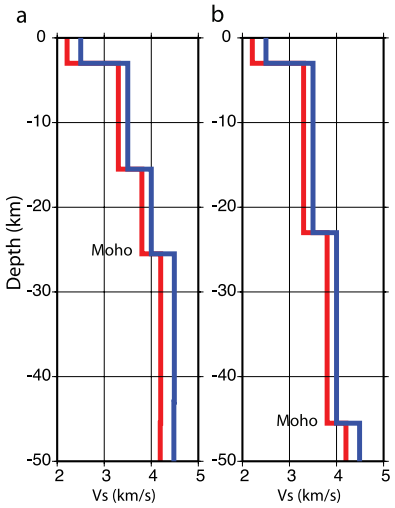

Figure 4. Initial models used in the inversion at each station. (a) Two initial velocity profiles with a 25-km crustal thickness. (b) Two initial velocity profiles with a 45-km crustal thickness. These low and high values for crustal thickness bound the range observed previously in the study area. Values of Poisson's ratio of 0.27, 0.29, and 0.31 were used for each of the four displayed curves, resulting in a total of 12 initial velocity models at each station.

and 260 km depth, 10 km between 260 and 330 km depth, and 20 km below 330 km depth. *Dugda et al.* [2007] demonstrated that velocities at lithospheric depths trade off with velocities below ~190 km depth. Following their approach we forward modeled a range of fixed shear wave velocity profiles below 190 km depth to find the model that best fit the long-period group velocities from the Harvard global model [*Larson and Ekström*, 2001]. In agreement with *Dugda et al.* [2007], we found that a model for Ethiopia with shear wave velocities of 10% below PREM [*Dziewonksi and Anderson*, 1981] provided the best fit and we fixed the velocities below 190 km to these values in the inversion.

[16] For the top 190 km, we used 12 different starting velocity models (Figure 4) in our inversions to investigate the sensitivity of our model results to starting crustal velocity, crustal thickness, and Poisson's ratio. These included distinct combinations of models with two possible crustal velocity profiles (Figure 4), two different values of crustal thickness (25 and 45 km) that bracket the published range of crustal thicknesses across Ethiopia, and three Poisson's ratios of 0.27, 0.29, and 0.31 (corresponding to Vp/Vs ratios of 1.78, 1.84, and 1.91). Figure 5 shows results for station DMRK demonstrating our method and representative results. In an earlier phase of testing, we tested starting models both with and without sedimentary basins, but found that for many stations inversions using starting models without sedimentary basins were unstable whereas those with basins were stable at all stations. We also tested a broader range of Poisson's ratios before settling on the three values from 0.27 to 0.31, which were chosen to limit the number of initial models needed while still providing values representative of the range reported in Ethiopia by *Dugda et al.* [2005] and *Stuart et al.* [2006].

4. Testing

4.1. Sensitivity Testing

[17] To test the sensitivity of our models, we used a range of input parameters including the initial velocity and Poisson's ratio models as described above and a range of influence parameters (weighting the relative influence of receiver function data to dispersion data) at each station.

[18] For two stations we also used a bootstrapping method to determine the uncertainty in our inversions due to scatter in the data, one on the Ethiopian Plateau with a low-velocity lower crust and another on the northeastern shoulder with a higher-velocity lower crust. In the bootstrapping, for a given station we conducted n sets of inversions, where n is the total number of receiver functions for that station. In each inversion set for the selected station, we randomly selected n receiver functions from the total of n. By randomly selecting, we allow the same trace to be selected multiple times and other traces to not be used. We then divided these randomly selected n traces into the proper ray parameter and frequency groups and stacked each group. We inverted this new set of stacks using each of 12 input velocity and Poisson's ratio models and a range of influence parameters (0.3, 0.5, and 0.7), and repeated for each of n sets of new stacks. At the station DMRK, this resulted in nearly 3000 inversions for the single station. Because of the intense computing requirements, we only inverted two stations using this method. The tight clustering of the resulting profiles (Figure 6) provides confidence in our models at the other stations and in our interpretations. We estimate that our total uncertainty in velocity is ~0.1 km/s in the lower crust and 0.2 km/s in the mantle, and the uncertainty in the depth to discontinuities is about 2.5 km in the crust and

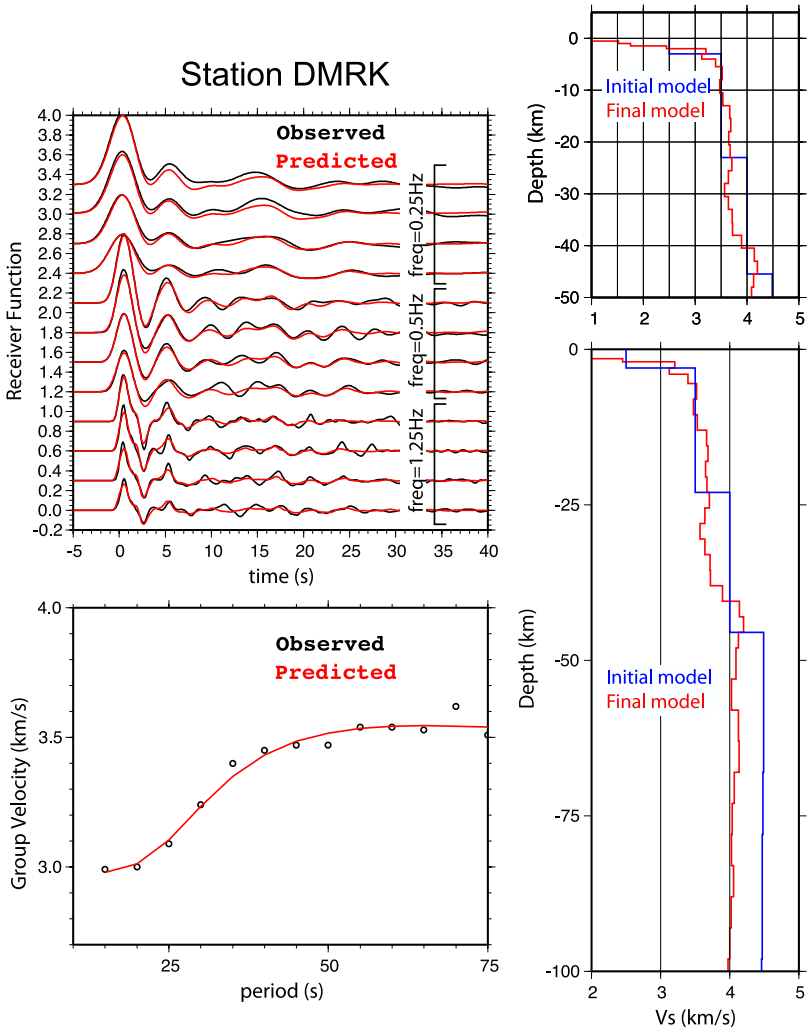

Figure 5. Representative results showing input receiver functions and dispersion curve (black) and synthetic fits from the final model (red). Receiver functions are offset along the vertical axis for plotting purposes. The receiver functions consist of three frequency bands (bracketed), with the four ray parameter groups for each frequency band plotted from low (bottom) to high (top) in each frequency bracket. The ray parameter bins used were 0.04–0.049, 0.05–0.059, 0.06–0.069, and 0.07–0.079. The dispersion curve is taken from the model of *Pasyanos* [2005].

uppermost mantle (the thickness of our layers in this depth range).

4.2. Comparison of Inversion Results With Active Source Crustal Profiles

[19] The proximity of the EAGLE broadband stations to active source wide-angle profiles from the EAGLE experiment allowed us to independently confirm the reliability of our joint inversion results within the crust. Figure 7 shows active source models along and across the MER [*Maguire et al.*, 2006], with 1-D profiles from our joint inversion located less than 15 km from the 2-D line (in most cases located directly along the 2-D line) overlain. Our results are very consistent with the active source modeling in discontinuity structure (depths to interfaces). A strong correlation is evident for the transition from low-velocity, near-surface layers to higher-velocity (~6 km/s) layers, for the midcrustal discontinuity at 10–20 km depth, and at the Moho. The intracrustal reflector modeled in the active source profile at 20–30 km depth along the across-axis line (Figure 7a) is not visible in our profiles as a velocity increase and at several stations is more consistent with the top of a lower crustal low-velocity zone. Very little change in velocity is modeled across this interface in the active source profiles. The discrepancy between our joint inversion results and the active source discontinuity at this level may be a result

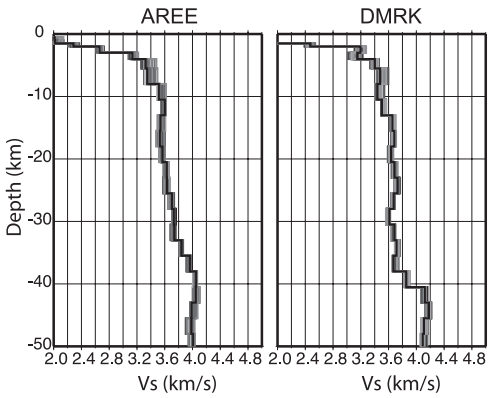

Figure 6. Results of bootstrap inversions at stations AREE (within the Northern MER) and DMRK (on the NW shoulder). The inversions test the sensitivity of the method to variations in inversion parameters, including 12 distinct starting models with varying velocity and Poisson's ratio, different groups of input data, and three different weighting parameters between receiver functions and surface waves (see text). The tight clustering of the output inversions in the lower crust shows the low sensitivity of the inversion to these parameters. The greater spread in the output models in the upper crust (above 10 km) may represent greater heterogeneity in the upper crust, as different groups of receiver functions include receiver functions from different events which travel different paths and therefore sample different geologic features. The low sensitivity of the inversions to the weighting parameter between receiver functions and surface waves indicates that while the surface wave data provide a smooth velocity function, the receiver functions provide most of the structure in the output inversion. The color of the line represents the RMS fit of that model to the data, with the black line providing the best RMS fit and lighter shades of gray progressively worse.

of the different sensitivities of the methods: wide-angle refraction studies have little sensitivity to low-velocity zones, whereas our joint inversion has equal sensitivity to velocity changes of either polarity.

[20] A significant difference between the results of the active source profiling and the passive source seismic studies is the presence or absence, respectively, of a high-velocity lower crustal layer. Although on the active source profile in Figure 7 the lower crust beneath the NW shoulder includes a 10-km-thick high-velocity lower crustal layer, for a total crustal thickness of ~50 km [*Mackenzie et al.*, 2005], results from *Dugda et al.* [2005, 2007], *Stuart et al.* [2006], and our joint inversion results show that this high-velocity body is a localized feature not characteristic of the NW shoulder, which more typically has a thickness ranging from 38 to 42 km. In the previous studies with Moho depths incompatible with those from the active source study [e.g., *Dugda et al.*, 2005; *Stuart et al.*, 2006] the source of the discrepancy between the results of the different methods was unclear. Our 1-D profiles, with both widespread coverage beneath the NW shoulder and information on the seismic velocity structure of the crust and upper mantle, can spatially map the lower crustal feature evident in the active source data. Velocity profiles from stations near the active source line beneath the NW shoulder show a distinctly different Moho gradient than the remaining stations (Figure 8). The anomalous stations in Figure 8b show a gradually increasing seismic velocity at the base of the crust over ~10 km, approximately the thickness of the underplate modeled by *Mackenzie et al.* [2005]. Away from these three stations the Moho is a sharper contrast (Figure 8c) and our crustal thickness estimates are in agreement with crustal thickness estimates from *Stuart et al.* [2006] and *Dugda et al.* [2005]. The anomalous thickness values of *Mackenzie et al.* [2005] appear to reflect a local crustal thickening and possible underplating. The cause of this thickening is unknown but we note that the active source line was placed to cross the western boundary of the rift in this location to take advantage of the gentle relief and monocline associated with the intersection of the Yerer-Tullu Wellel Volcanotectonic Lineament and the NMER, both volcanically active, and perhaps the enhanced crustal underplating is related to this intersection of two rift trends.

5. Results

[21] Results for our joint inversion are shown in Figures 9–12. Thirty-nine stations from the EAGLE and EBSE networks were used for our final inversions. In Figure 9, stations are grouped by domains on the basis of the discussion by *Keranen and Klemperer* [2008] and as summarized in section 2. Our results for crustal thickness, lower crustal shear wave velocity, and upper mantle shear wave velocity are summarized in Table 1.

[22] Beneath the NW shoulder, the Moho depth range is from 38 to 41 km, whereas beneath the SW shoulder Moho depth ranges from 33 to 36 km (Figure 10). Beneath the NMER, crustal thickness ranges from 28 to 36 km thick. To the south in the CMER, crustal thickness for AMME, the one station available to us within the CMER proper, is 38 km. Crustal thickness beneath the eastern shoulder is 38–41 km (Figure 10). Our crustal

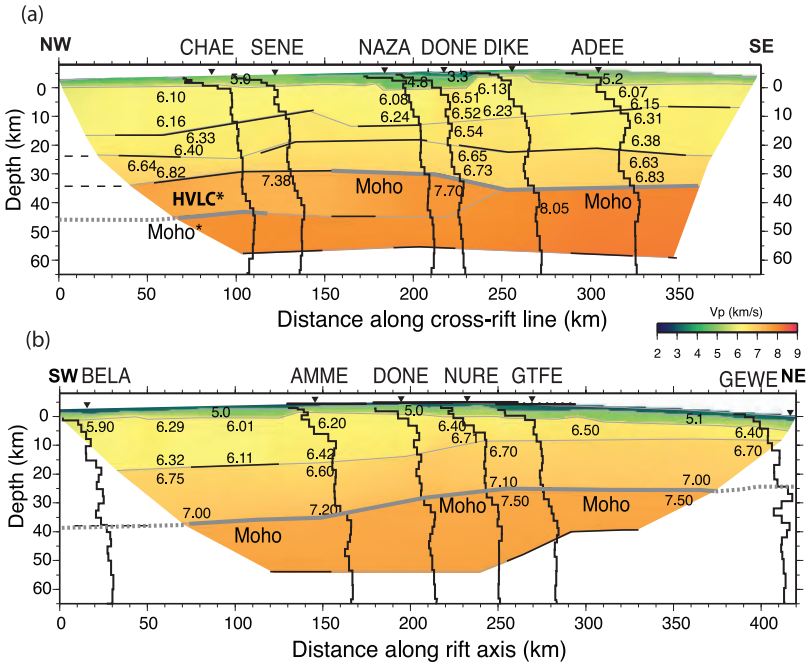

Figure 7. Comparison of joint inversion shear wave velocity results (Vs) for stations located near active source profiles with active source 2-D modeling results (Vp) from *Maguire et al.* [2006]. (a) Comparison to cross-rift line. (b) Comparison to along-axis line. The depth to major boundaries, such as the Moho and intracrustal reflectors, matches closely between the two sets of results. Numbers on the profiles are modeled Vp velocities from active source modeling. Because of the uncertainty in converting from Vs to Vp (or vice versa) with only whole-crustal Vp/Vs ratios available from independent analyses [*Dugda et al.*, 2005; *Stuart et al.*, 2006], we have not tried to compare absolute velocity. The HVLC (high-velocity lower crust) modeled in the active source profile along line 1 in Figure 7a is not a feature characteristic of the NW shoulder and is spatially very localized (Figure 8). The depth to Moho beneath the NW shoulder is ~40 km [from *Stuart et al.*, 2006; *Dugda et al.*, 2005; this study]. Accordingly, we refer to the HVLC body and the Moho as observed on the wide-angle profile beneath the NW shoulder as HVLC* and as Moho*.

thickness estimates are in good agreement with the results reported by *Dugda et al.* [2005] and *Stuart et al.* [2006] using the *Zhu and Kanamori* [2000] receiver function stacking technique.

[23] The uppermost mantle shear wave velocity in our results is similar to that found by *Dugda et al.* [2007] and ranges between 4.0 and 4.3 km/s (Figure 11). These values are low with respect to

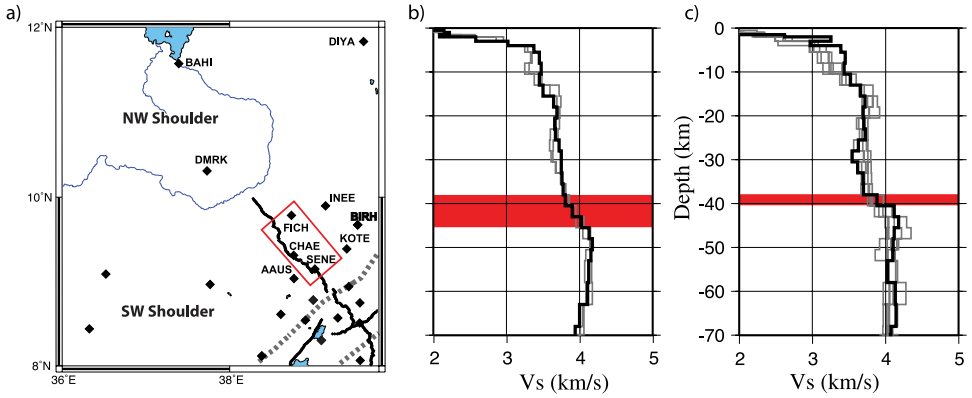

Figure 8. (a) Map of stations on the NW shoulder. Unnamed stations are south of the YTVL on the SW shoulder. (b) Profiles from the NW shoulder at the stations within the red rectangle in Figure 8a, an area on the NW shoulder with an anomalous lower crustal velocity gradient rather than a sharp Moho. (c) Shear wave velocity profiles from the NW shoulder at named stations outside of the red rectangle in Figure 8a, showing a sharp Moho boundary at ~40 km.

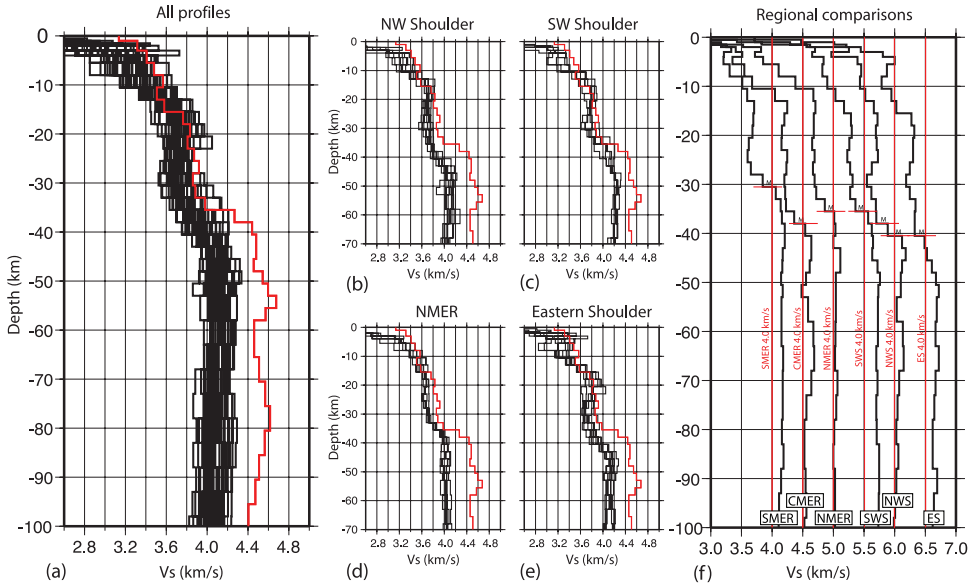

Figure 9. Profiles of our joint inversion results. (a–e) The red profile is the joint inversion result for KIBE [*Julia et al.*, 2005], a station located along-strike in the Mozambique Belt in Tanzania (location shown in Figure 1). The profile from KIBE is representative of the shear wave velocity structure of the lithosphere surrounding the EARS to the south. (f) A comparison of representative curves from each region with the Moho identified with a horizontal red bar. The curves are offset along the horizontal axis for plotting purposes; the vertical red bars identify the 4.0 km/s line for each profile.

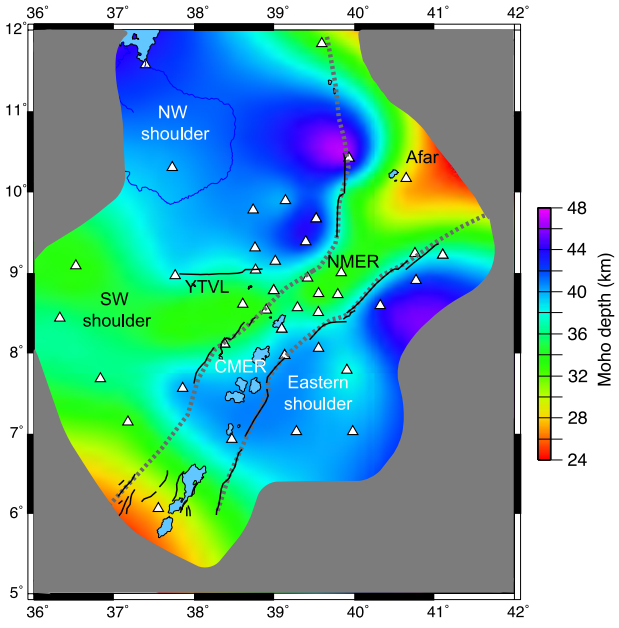

Figure 10. Contour map of Moho depth from our joint inversion results. The dashed gray lines show the rift outlines. Solid black lines are the rift border faults. White triangles are the stations we utilized from the EAGLE and EBSE networks. Crustal thickness beneath the rift shoulders is generally ~40 km, with the exception of the SW shoulder, which has a thickness of ~35 km. Crustal thickness within the NMER is ~35 km and within the CMER is 38–40 km (from this study and previous studies).

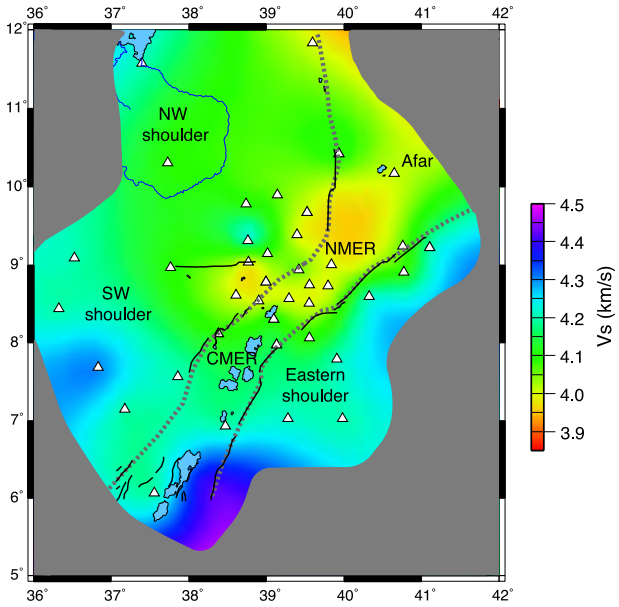

Figure 11. Contour map of uppermost (average of the top 5 km) mantle shear wave velocity from our joint inversion results. Symbols as in Figure 10. The SW shoulder has the highest observed upper mantle Vs within our study area (4.2–4.3 km/s), the eastern and NW shoulder have velocities of 4.0–4.2 km/s, and the NMER/YTVL has the lowest upper mantle velocity, 4.0 km/s. Uppermost mantle velocity in the PREM model is 4.5 km/s.

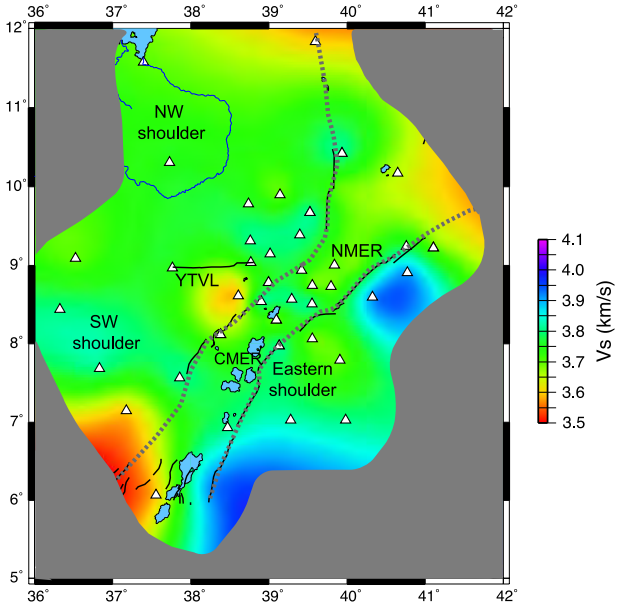

Figure 12. Contour map of lowermost (average of the lower 5 km) crustal shear wave velocity from our joint inversion results. Symbols as in Figure 10. The shear wave velocity of the lower crust in our study area is 3.6–3.8 km/s across nearly the entire region, with only two stations in the study area having a lower crustal velocity of 3.9 km/s. The shear wave velocity of the lower crust along-strike in the Mozambique Belt to the south is 3.9–4.1 km/s [*Julia et al.*, 2005].

4.5 km/s in the uppermost mantle in the PREM model and in Tanzania and Kenya away from the Cenozoic rift [*Julia et al.*, 2005]. Upper mantle velocity differs between domains within Ethiopia, with values of 4.0–4.2 km/s beneath the NW shoulder, 4.2–4.3 km/s beneath the SW shoulder, 4.0–4.1 km/s beneath the NMER, and 4.1 km/s beneath the eastern shoulder (Figure 11). The region with the lowest upper mantle seismic velocity (~4.0 km/s) in the 5 km below the Moho is the NMER and the YTVL (Figure 11), which lies above the lowest upper mantle seismic velocity at 75 km depth [*Bastow et al.*, 2005]. However, in our inversion a similar low-velocity anomaly is not seen beneath the CMER despite its observation at 75 km depth using travel time tomography [*Bastow et al.*, 2005], either a result of a dipping low-velocity zone or reflecting the lower amplitude of the CMER low-velocity zone in the upper mantle tomography. The 20–40 km thick mantle lid visible on profiles from the Western Ethiopian Plateau in the work by *Dugda et al.* [2007, Figure 6, line A-A'] is located beneath the SW Ethiopian Plateau. The mantle lid is present in our results from the SW plateau (Figure 9) but is not evident beneath the NW plateau, where the upper mantle Vs is lower.

[24] Perhaps the most notable result of our inversions is the identification of a widespread, low-velocity lower crust throughout the region of flood basalt volcanism (Figure 12). In contrast to the marked contrast between rift and plateau structure of the EARS in Kenya [*Dugda*, 2007], the velocity structure of the crust and uppermost mantle in the MER is very similar to the velocity structure beneath the NW Ethiopian Plateau (Figure 9).

Table 1. Lower Crustal Shear Wave Velocity, Upper Mantle Shear Wave Velocity, and Crustal Thickness for Each Station in Our Joint Inversion[a]

Station	LC Velocity (km/s)	UM Velocity (km/s)	H (km)
AAUS	3.75	4.0	38.0
ADEE	3.7	4.2	38.0
ADUE	3.8	4.0	33.0
AMME	3.7	4.1	38.0
ARBA	3.6	4.2	28.0
AREE	3.75	4.1	35.5
ASEE	3.8	4.2	40.5
BAHI	3.7	4.2	43.0
BEDE	3.9	4.1	43.0
BELA	3.8	4.2	40.5
BIRH	3.8	4.0	43.0
BORE	3.7	4.0	33.0
CHAE	3.8	4.2	40.5
CHEF	3.9	4.4	33.0
DELE	3.8	4.2	35.5
DIKE	3.6	4.1	40.5
DIYA	3.6	4.0	33.0
DMRK	3.75	4.2	40.5
DONE	3.8	4.0	35.5
DZEE	3.75	4.0	35.5
GEWE	3.65	4.0	28.0
GOBA	3.8	4.2	40.5
GTFE	3.7	4.1	33.0
GUDE	3.75	4.2	38.0
HIRN	3.7	4.2	38.0
HOSA	3.8	4.2	40.5
INEE	3.7	4.3	40.5
JIMA	3.8	4.3	35.5
KARA	3.8	4.1	45.5
KOTE	3.8	4.2	43.0
LEME	3.6	4.0	33.0
MECE	3.9	4.2	43.0
NAZA	3.8	4.0	35.5
NEKE	3.7	4.1	33.0
NURE	3.7	4.0	35.5
SELA	3.8	4.1	40.5
SHEE	3.7	4.0	35.5
TERC	3.6	4.2	33.0
WASH	3.7	4.0	35.5

[a] LC, lower crustal; UM, upper mantle; H, crustal thickness.

The results from our inversion show that the lower crustal velocities beneath the MER (~3.7 km/s), the NW shoulder (~3.8 km/s), and the region of the eastern shoulder covered by flood basalt volcanism (~3.8 km/s) are all reduced by 0.2–0.4 km/s (Figure 12) from velocities in the lower crust in the along-strike Mozambique Belt in Tanzania [*Julia et al.*, 2005]. The largest difference between the crust and upper mantle profiles from the MER and NW Plateau is the ~5 km difference in crustal thickness. This thinning is caused by upper crustal and mid-crustal thinning within the rift valley itself, modeled in the across-axis wide-angle seismic refraction line from the EAGLE experiment [*Mackenzie et al.*, 2005; *Maguire et al.*, 2006], rather than by differences in lower crustal thickness.

6. Interpretation of Low Shear Wave Velocity in the Upper Mantle and Lower Crust

6.1. Upper Mantle Shear Wave Velocity of 4.0–4.2 km/s

[25] The primary potential causes of low upper mantle shear wave velocity are composition, increased temperature, the presence of fluids (such as partial melt), grain size reduction [*Faul and Jackson*, 2005], or some combination of these factors. These factors can be analyzed individually to assess the possible contribution of each to the low observed upper mantle shear wave velocity.

[26] Composition and grain size can be eliminated as predominant effects because of the large magnitude (5–10%) of the observed decrease. The composition of the mantle is less variable than the composition of the crust, and at most compositional variations cause an ~1% change in shear wave velocity [*Cammarano et al.*, 2003]. The effect of changing the grain size from 1 cm to 1 mm, the range commonly estimated for the upper mantle [*Hirth and Kohlstedt*, 2003, and references therein], results in an ~100 m/s (~2%) change in velocity at 1200°C (Figure 13), again not enough to account for the 300–500 m/s decrease observed in Ethiopia.

[27] We next examine the remaining factors: increased temperature and partial melt. These two factors are likely interdependent and combine to reduce the shear wave velocity. With the two effects superimposed, it is difficult to constrain the exact contribution from each. We instead seek to develop reasonable maxima and minima for each factor. Two recent publications [*Faul and Jackson*, 2005; *Priestley and McKenzie*, 2006] discuss the relationship between upper mantle temperature and shear wave velocity. The behavior of these two models differs (Figure 13), however both predict that an upper mantle temperature over 1300°C is required to produce a shear wave velocity of 4.1 km/s or lower, and that above 1300°C dVs/dT increases rapidly. On the basis of *Faul and Jackson* [2005] and *Priestley and McKenzie* [2006], if there is no contribution from partial melt, the estimated temperature of the upper mantle for seismic velocity ranging from 4.0 to 4.1 km/s (i.e., beneath the MER and NW plateau) is predicted to be 1300–1350°C. To consider the effect of only partial melt with no increase in temperature, we use the estimate of *Faul et al.* [1994] of a 3.3% reduction in seismic velocity per percent melt. In this melt-only case, 3% melt is required in the upper mantle to reduce the seismic velocity by the observed 10 percent.

[28] Both high temperature and partial melt are capable of reducing the seismic velocity of the upper mantle. It is implausible however to assume that one of these effects would be present without the other. This is evident in the experimental results of *Hirschmann et al.* [1998]. The authors measured percent melt produced as a function of increasing temperature for upper mantle peridotites, including a peridotite composition similar to that present in Ethiopian xenoliths [*Conticelli et al.*, 1999] (Figure 14). As Figure 14 demonstrates, as upper mantle temperature increases above ~1270°C there is a rapid increase in the percent partial melt present from near zero to ~5%. If a temperature of the uppermost mantle of 1300°C is required to reduce shear wave velocity to 4.1 km/s by a purely thermal effect as discussed above, we see that at this temperature ~5% partial melt would be present (further reducing seismic velocity). The combined effect of high temperature and partial melt would then lower the shear wave velocity below that observed in Ethiopia.

[29] Thus the high temperature that would be required to account for the observed low seismic velocity cannot be present without a contribution from partial melt. In contrast, in principle the observed seismic velocity reduction could be the effect of transient partial melt without anomalous upper mantle temperature. To constrain the lower bound on the upper mantle temperature, we consider independent evidence regarding the thermal structure. Although we lack heat flow data in our

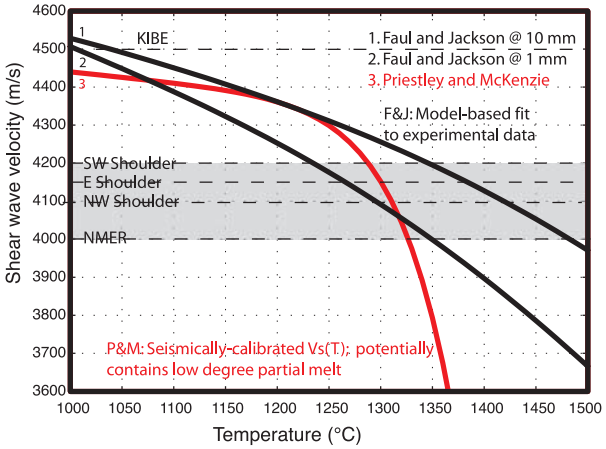

Figure 13. Estimated shear wave velocity versus temperature in the upper mantle from *Faul and Jackson* [2005] and *Priestley and McKenzie* [2006]. The two curves from the *Faul and Jackson* [2005] model are for upper mantle grain sizes of 1 and 10 mm. The gray box represents the range of shear wave velocity values observed beneath the MER and the adjacent plateaus. The horizontal dashed black lines show the average upper mantle temperature for the different regions discussed in the text. For comparison, the upper mantle temperature at KIBE is ~4.5 km/s, which corresponds to a temperature much less than 1000°C for the *Priestley and McKenzie* [2006] model, which may be the more accurate of the two curves in this temperature range given that the *Faul and Jackson* [2005] model is only calibrated for temperatures between 1000°C and 1300°C. The two models show different behavior, but for a velocity of 4.1 km/s both predict an upper mantle temperature of ~1300°C.

study area, mantle xenoliths found in Oligocene and Quaternary basalts near Lake Tana on the Ethiopian Plateau [*Conticelli et al.*, 1999] from a depth range of 40–50 km can be used as estimates of the temperature of the uppermost mantle at the time of eruption. These studies indicate minimum upper mantle temperatures between 920 and 1045°C for the Oligocene and Quaternary samples. This temperature is well above a steady state continental geotherm [*Chapman*, 1986]. We conclude that the uppermost mantle temperature is elevated by over several hundred degrees above stable continental regions, and that the observed seismic velocity reduction is the result of both high temperature and partial melt. We conclude that the most likely lower bound for the temperature is ~1250°C, where melt begins to form [*Hirschmann et al.*, 1998], and the most likely upper bound is ~1300°C (at which the amount of melt produced would create a velocity effect greater than that permitted by observations). This temperature range is compatible with a melt percent of up to 3%. The cause of the high temperature in the uppermost mantle is interpreted to be the thermal perturbation associated with the Afar plume. The strong evidence from previous geophysical and geochemical studies for a thermal perturbation in the mantle down to depths of 600 km is summarized in section 1. *Dugda et al.* [2007] model instantaneous thinning of the lithosphere due to plume impingement at the time of the flood basalt volcanism (~30 Ma), with hot plume material remaining to the present. Their models show that the temperature increase (still present today) resulting from the transfer of heat from the plume material to the lithosphere is enough to account for the observed reduction in shear wave velocity [*Dugda et al.*, 2007].

6.2. Lower Crustal Shear Wave Velocity of 3.7–3.8 km/s

[30] Unlike the upper mantle, where possible compositional effects on seismic velocity are small relative to the observed velocity reduction [*Cammarano et al.*, 2003], in the crust one would commonly assume that the observed lower crustal velocity decrease (to 3.7–3.8 km/s) implies a felsic lower crust. In the following discussion we instead show that the composition is unlikely to be felsic and that the low velocity in the lower crust is most likely the result of a combination of high temperature and partial melt as in the upper mantle.

[31] Little information on the temperature of the lower crust is available for Ethiopia. Interpreting temperature from seismic velocity in the lower

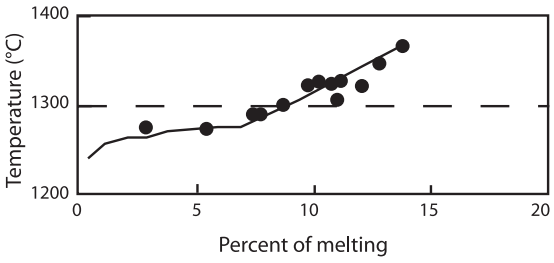

Figure 14. Experimental results for percent melt versus temperature for depleted peridotite, modified from *Hirschmann et al.* [1998] by permission of Oxford University Press. At 1300°C (our upper bound on temperature if the low upper mantle shear wave velocity below Ethiopia is caused only by high temperature), melt percent would be over 5% on the basis of these experimental results. Black circles are reported measurements, and the solid black line is the predicted curve using the MELTS algorithm.

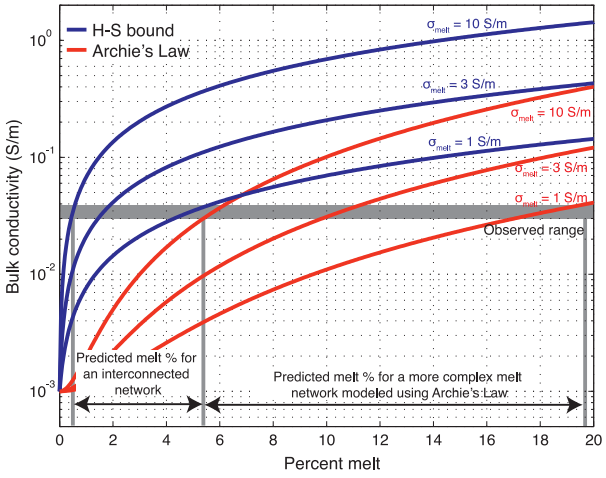

Figure 15. Constraints on the amount of melt present in the lower crust in Ethiopia from observed conductivity values of *Whaler and Hautot* [2006]. Blue curves are calculated using the upper Hashin-Shtrikman bounds, which assumes a connected melt network and provides a lower bound on the amount of melt present. Red curves are calculated using the modified version of Archie's Law for materials containing partial melt [*Hermance*, 1979] for a matrix conductivity of 0.001 S/m and melt conductivities of 1, 3, and 10 S/m. Between 0.5% and 5% melt is present in the lower crust using the H-S upper bound, and between 6% and 20% melt is present using the modified form of Archie's Law.

crust is difficult because the value of dVs/dT at high temperatures (>600°C) for crustal lithologies is not well constrained. For temperatures up to 600°C (still significantly below that plausible for the Ethiopian lower crust based on the previous arguments for a 1250–1300°C upper mantle) *Kern et al.* [2001] show an average of ~0.21 m/s/K decrease in shear wave velocity as temperature increases. Using a value of 0.21 m/s/K for dVs/dT requires a temperature increase of 1000–2000°C above that of the lower crust in Kenya (~1500–2500°C) to create the observed decrease of 0.2–0.4 km/s. That temperature range is clearly unrealistic, likely because the dVs/dT value at lower temperatures is not applicable for higher temperatures. *Kampfmann and Berckhemer* [1985] show a sudden decrease in the shear wave modulus at ~800°C for mafic rocks, which would cause dVs/dT to rapidly increase above 800°C. Without better constraint on dVs/dT we are unable to quantitatively convert observed seismic velocity in the lower crust to temperature, but using either the *Kern et al.* [2001] results or the *Kampfmann and Berckhemer* [1985] results, the temperature in the lower crust is predicted to be 800°C or greater. A hot lower crust is also consistent with extrapolation of the predicted anomalously high upper mantle temperature.

[32] An independent constraint on the state of the lower crust comes from electrical conductivity data collected along a cross-rift line (Figure 2) by *Whaler and Hautot* [2006]. These data indicate a strong similarity in crustal structure between the NMER and the NW Ethiopian Plateau; the resistivity structure beneath the NMER and the Ethiopian Plateau is nearly the same (as are the seismic velocity profiles) with lower crustal conductivity of $\sim 4.10^{-2}$ S/m. In contrast the Somali Plateau shows a lower conductivity, below 1.10^{-2} S/m. The integrated lower crustal conductivity (conductance) beneath the rift and the NW Ethiopian Plateau is at least 400 S (siemens), the average conductance for Phanerozoic lower crust, while the conductance below the Somali Plateau is only ~100 S [*Whaler and Hautot*, 2006]. High electrical conductivity in the lower crust implies saline fluids, graphite, or melt. Although we cannot a priori rule out any of these, the high temperatures implied by the previous discussion suggest anhydrous equilibrium conditions and the recent magmatism makes melt the natural explanation. If we make the assumption that melt is present in the lower crust and causes the high observed conductivity, we can constrain the amount present beneath the Ethiopian Plateau using the observed conductivity values [e.g., *Schilling et al.*, 2006] independent of seismic velocity.

[33] Because of the large difference in the conductivity of basaltic melt (up to 10 S/m) and solid rock (<0.01 S/m) [*Roberts and Tyburczy*, 1999], electrical conductivity is very sensitive to melt percent. This electrical conductivity can be modeled using the Hashin-Shtrikman bounds [*Hashin and Shtrikman*, 1962], with the upper bound describing an ideal, connected melt network. This bound will describe the lower limit on the amount of melt present. The lower Hashin-Shtrikman bound describes isolated melt pockets and limits the maximum amount of melt present. If we model the upper Hashin-Shtrikman bounds using melt conductivity values of 1 S/m, 3 S/m, and 10 S/m, using a matrix conductivity of 0.001 S/m, we predict a melt percent between 0.5 percent (melt conductivity of 10 S/m) and 5 percent (melt conductivity of 1 S/m) as the lower bound on melt present (Figure 15). This assumes the ideal case of interconnected melt pathways. If some of the melt is present in isolated pockets the melt percent required to produce the observed bulk conductivity is higher. Archie's Law is a reasonable way to estimate a more complex melt system

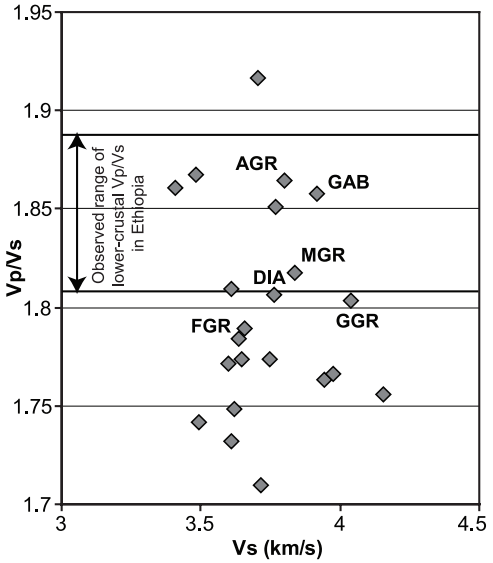

Figure 16. Vp/Vs ratio versus Vs (km/s) at room temperature and 800 MPa for different rock types using data from *Christensen* [1996]. Vs as shown is higher than expected in the lower crust since data are not temperature-corrected, but Vp/Vs has little dependence on temperature. MGR, mafic granulite; DIA, diabase; GGR, mafic garnet granulite; FGR, felsic granulite; GAB, gabbro. The range of observed lower crustal Vp/Vs values in Ethiopia, calculated using our joint inversion results for Vs and active source Vp profiles, is shown by the horizontal black lines. The Vp/Vs ratio of felsic granulite is lower than the range of observed values in Ethiopia. The Vp/Vs ratio of mafic granulite, present in the lower crust both to the north in the Arabian Shield and to the south in Tanzania, lies within the observed range.

between the Hashin-Shtrikman end-members of completely isolated and completely connected networks [*Hermance*, 1979; *Merzer and Klemperer*, 1992]. If we use this method assuming a complex melt system [*Hermance*, 1979], we estimate between 6% and 20% melt in the lower crust (Figure 15) rather than 0.5 to 5% estimated for ideally interconnected pathways. The presence of melt in the crust beneath the NW plateau away from the MER is supported by elevated bulk crustal Vp/Vs ratios up to 1.9 [*Dugda et al.*, 2005; *Stuart et al.*, 2006]. A Vp/Vs ratio of 1.9 is commonly taken to represent a contribution from melt [e.g., *Menke et al.*, 1998]. This lower crustal melt that we infer is not only present beneath the MER, it is present beneath the entire Ethiopian Plateau even hundreds of kilometers from the rift valley. The plateau has been the location of extensive off-axis Mio-Pliocene and Quaternary volcanism [*Abate et al.*, 1998; *Conticelli et al.*, 1999], possibly reflecting this continued presence of melt far from the rift axis.

[34] As a final possibility, a lower crust of felsic granulite across the entire region could cause the lower crust to have a shear wave velocity of ~3.7 km/s [*Christensen*, 1996]. Such a composition, however, is unlikely. Mafic lower crustal xenoliths are described for both the Arabian-Nubian Shield to the north [*McGuire and Stern*, 1993; *Al-Mishwat and Nasir*, 2004] and along the trend of the Mozambique Belt to the south [*Mansur et al.*, 2006]. These terranes meet in Ethiopia, therefore one might expect that the Ethiopian lower crust is composed of a similar mafic lithology. Vp/Vs ratios provide a stronger constraint on composition than either Vp or Vs alone. Vp/Vs ratios in Ethiopia have previously been estimated for the whole crust using the Zhu and Kanamori receiver function stacking method [*Dugda et al.*, 2005; *Stuart et al.*, 2006], but are estimated here for just the lower crust by using the ratio of the lower crustal shear wave velocity measured in our inversions to the lower crustal compressional wave velocity modeled using wide-angle data [*Maguire et al.*, 2006]. The Vp/Vs ratio for the lower crust in Ethiopia ranges from 1.81 to 1.88. As shown in Figure 16, felsic granulite has a Vp/Vs ratio of 1.79, lower than that observed in Ethiopia, and mafic granulite has a Vp/Vs ratio of 1.82, within our observed range.

[35] The regional mafic lower crustal xenoliths and the observed Vp/Vs ratios cannot absolutely eliminate a felsic lithology in the lower crust as the cause of the low observed lower crustal shear wave velocity in Ethiopia. However, with strong evidence for (1) high temperature causing the upper mantle low-velocity anomaly (section 6.1), which would conduct into the lower crust to reach thermal equilibrium; (2) strong evidence for the presence of melt in the lower crust from conductivity measurements (section 6.2); and (3) suggestions of a mafic lower crust from Vp/Vs ratios and along-strike lower crustal mafic xenoliths (section 6.2), it is quite unlikely that a felsic lower crust is responsible for the low observed shear wave velocities.

7. A Hot, Ductile Lower Crust and Upper Mantle With Partial Melt

[36] Additional lines of evidence support our interpretation of a hot, ductile lower crust with partial melt above a hot mantle lithosphere, also with partial melt. Geodetic observations indicate that extension between the Nubian and Somalian plates is distributed over a broader region than the 80–100 km width of the MER [*Bendick et al.*, 2006].

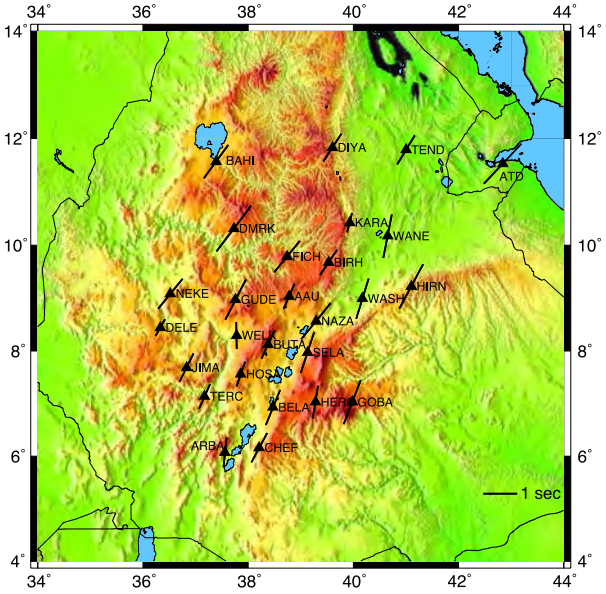

Figure 17. Shear wave splitting results across the MER and the Ethiopian Plateau modified from *Gashawbeza et al.* [2004]. Stations are represented by black triangles. The azimuth of the line at each station represents the azimuth of the fast direction of polarization of the shear wave. The length of the line is scaled according to the delay time between the arrivals in the fast and slow polarization directions, which is a measure of the integrated anisotropy below the station. Both the azimuth and the delay time remain relatively constant across the study area and are interpreted as reflecting the broad (~400-km-wide) distribution of melt not only beneath the rift but beneath the rift shoulders far from the surface structural expression of the rift.

The authors conclude that the high temperature and mechanical stretching in the MER create distributed, continuous extension in a viscous lower crust over a wide region [*Bendick et al.*, 2006]. If extension in the lower crust is broadly distributed but upper crustal extension is localized within the structural rift, lower crustal thickness should not change as much across our study region as upper crustal thickness. This can be tested by looking at the active source seismic profiles. As noted above, very little to no variation in lower crustal thickness is modeled in the profiles (if we exclude the modeled high-velocity lower crust beneath the NW shoulder for reasons discussed in section 4) either along or across the axis of the rift [*Maguire et al.*, 2006], further supporting distributed extension at this depth.

[37] Results from shear wave splitting studies [*Gashawbeza et al.*, 2004] (Figure 17) also support active deformation distributed far from the rift axis. In studies focused on the Ethiopian rift valley, observed splitting of similar magnitude and azimuth is interpreted to result from thin pockets of melt within the lithosphere aligned parallel to the rift [*Ayele et al.*, 2004; *Kendall et al.*, 2005]. The consistent delay times and azimuths of the fast polarization direction of splitting over the entire region of low lower crustal velocities extending hundreds of kilometers away from the rift itself (Figure 17) suggests that aligned pockets of melt may be present over this broad region, particularly when viewed in combination with the evidence for a hot upper mantle and lower crust over this same region. The previous interpretation of this data set uncritically assumed melt-filled cracks would only be present beneath the rift and so concluded that the uniformity of the splitting represented a Proterozoic lithospheric fabric [*Gashawbeza et al.*, 2004]. We do not exclude preexisting fabrics as a contributing cause of the observed splitting pattern, but on the basis of the additional evidence presented here we believe that melt-filled cracks likely contribute to the observed splitting far from the rift itself and a combination of the two effects is our preferred interpretation of the splitting results over the entire region. In addition to the studies described previously, upper mantle seismic tomography [*Benoit et al.*, 2006a; *Bastow et al.*, 2008] shows a broad thermal upwelling beneath the Ethiopian Plateau down to depths of at least 400 km that is laterally extensive for about 400 km, providing further support for an elevated thermal regime.

[38] The combination of low shear wave velocity, high lower crustal conductivity, and high upper mantle temperature makes high lower crustal temperature with the presence of partial melt beneath the MER and the NW Ethiopian Plateau the most reasonable interpretation for our observations of low shear wave velocity in the lower crust. The melt is likely present in aligned pockets perpendicular to the extension direction [e.g., *Ayele et al.*, 2004; *Kendall et al.*, 2005], as suggested by shear wave splitting measurements, although even our minimum estimate of melt percent from lower crustal electrical conductivities and upper mantle seismic velocities (0.5%; Figures 14 and 15) is far higher than the 0.1% suggested by *Ayele et al.* [2004] and *Kendall et al.* [2005]. Because melt fraction inferred from shear wave splitting relies on assumptions about crack aspect ratio, *Ayele et al.* [2004] and *Kendall et al.* [2005] simply chose the maximum plausible aspect ratio (100:1) to minimize the melt fraction required to explain their

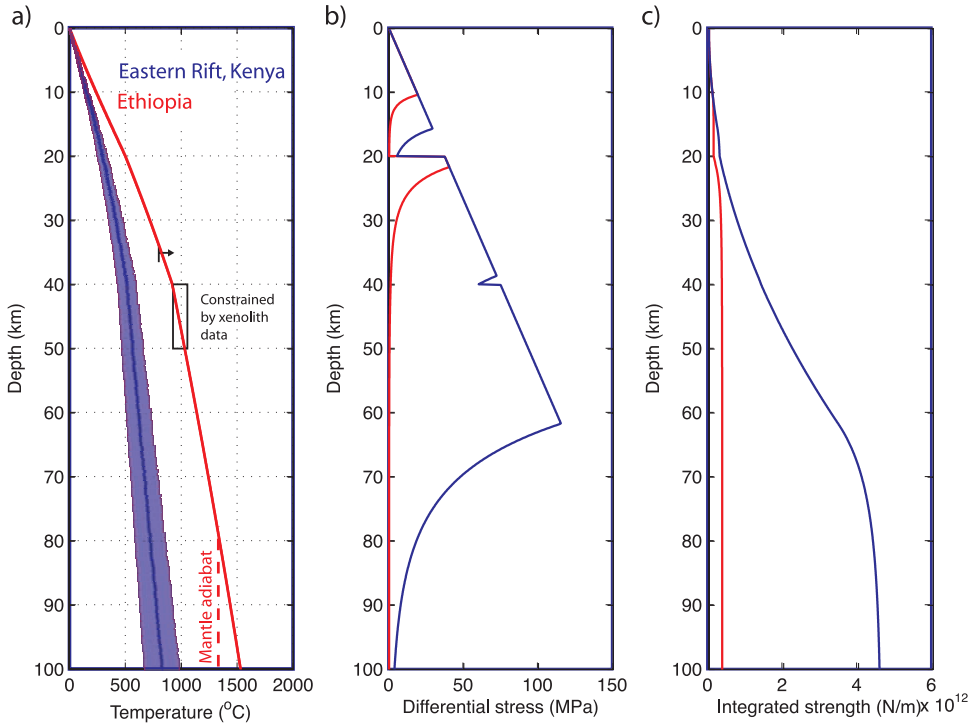

Figure 18. (a) Geotherms, (b) strength profiles, and (c) integrated strength of the lithosphere adjacent to the eastern branch of the East African Rift System (blue curves) and adjacent to the Main Ethiopian Rift (red curves) beneath the Ethiopian Plateau. In Figure 18a a range of temperature with depth is shown for the Eastern Rift; the central curve is used for the plots in Figures 18b and 18c. The integrated strength of the lithosphere (Figure 18c) surrounding the eastern branch is an order of magnitude higher than surrounding the Main Ethiopian Rift. See Table 2 for values used in the calculations of the geotherms (Figure 18a) and strength envelopes (Figures 18b and 18c). All values used for the Ethiopia and Kenya curves were the same with the exception of the surface heat flow, the range for which was taken from *Nyblade et al.* [1990] for Kenya and modeled using subsurface estimates of temperature for Ethiopia based on the xenolith data from *Conticelli et al.* [1999] as a constraint. In Figure 18a the vertical line and accompanying arrow in the lower crust for the Ethiopian curve indicate the temperature at which the shear modulus drops sharply [*Kampfmann and Berckhemer*, 1985] and dVs/dT increases. Our analysis indicates that the most likely cause for the observed low lower crustal shear wave velocity below 35 km is temperature, and therefore we are at or above this temperature in the lower crust in Ethiopia.

observations and the observations of *Gashawbeza et al.* [2004]. Simply reducing the crack aspect ratio to 20:1 fits the shear wave splitting data with the same (~ 90 km) partial melt layer thickness and our increased minimum (0.5%) melt fraction. Within the crust itself the melt appears to be more pervasive beneath the NMER than beneath the NW plateau on the basis of higher delay times in crustal shear wave splitting [*Keir et al.*, 2005] and higher values for Poisson's ratio within the rift itself [*Dugda et al.*, 2005; *Stuart et al.*, 2006].

8. Conclusions and Implications

[39] Our joint inversion of receiver function waveforms and surface wave dispersion curves in Ethiopia leads to the following conclusions:

[40] 1. The shear wave velocity of the upper mantle beneath Ethiopia is low (4.0–4.2 km/s) over an area ~400 km wide including both the Main Ethiopian Rift and the adjacent plateaus, ~0.3 km/s lower than the shear wave velocity of the rift margins elsewhere in the EARS.

[41] 2. The shear wave velocity of the lower crust across this same broad region is 3.7–3.8 km/s, ~0.3 km/s lower than the shear wave velocity of the lower crust elsewhere in the EARS.

[42] 3. The upper mantle immediately beneath the Moho is between 1250°C and 1300°C with up to 4% melt. The lower crust has between 0.5% and 20% melt (assuming a fully interconnected melt network and a more complex melt network, respectively) over a region much broader (~400 km) than the ~20 km wide zone of active intrusion

Table 2. Parameters Used in the Calculation of the Geotherms and Strength Envelopes in Figure 18 for Rift Shoulders in Ethiopia and Kenya[a]

	Ethiopia	Kenya
Surface heat flow (mW/m^2)	67*	43–51
Upper crustal conductivity (W/m/K)	3	3
Lower crustal conductivity (W/m/K)	2.0	2.1
Upper crustal heat production (W/m^3)	1e-6	1e-6
Lower crustal heat production (W/m^3)	1e-7	4e-7
Thickness of upper crust (km)	20	20
Moho depth (km)	40	40
Strain rate (1/s)	1e-15	1e-15

[a] Range of heat flow for Kenya from *Nyblade et al.* [1990]; heat flow listed for Ethiopia is estimated on the basis of the heat flow required to match temperature constraints at depth using selected values for other parameters. Moho depth is based on the average depth beneath the eastern and northwestern shoulders, thickness of the upper crust is from active source modeling [*Maguire et al.*, 2006], and strain rate is from both GPS [*Bendick et al.*, 2006] and crustal thinning estimates for Ethiopia. Values for the remaining thermal parameters are from *Artemieva and Mooney* [2001]. Strength curves assume power law failure for granite, mafic granulite, and peridotite for the upper and lower crust and upper mantle, respectively [*Ranalli*, 1997].

within the MER [*Keranen et al.*, 2004] or the ~100 km wide rift valley.

[43] 4. Strain in the lower crust is spread over the ~400 km region with low lower crustal and upper mantle shear wave velocities, more broadly distributed than strain in the upper crust (localized within the ~100 km wide rift).

[44] 5. The MER is an example of a "narrow" rift forming in hot continental lithosphere.

[45] The MER is traditionally considered to have developed in initially thick, strong cratonic lithosphere. Previous studies [*Buck*, 1991; *Brun*, 1999] have demonstrated that the narrow rift mode preferentially evolves in cool, thick lithosphere with high depth-integrated strength. Here we show that this condition is unlikely for the MER, and that the rift instead appears to have developed in a region with a weak and ductile lower crust and hot upper mantle. The limits of the thermally modified lithosphere closely follow the limits of the Ethiopian flood basalt province (Figure 1). Plume impingement at ~30 Ma led to the rapid thinning of the lithosphere and the subsequent transfer of heat from the plume material to the crust and upper mantle [*Dugda et al.*, 2007].

[46] We have shown that the Ethiopian lithosphere was likely hot and weak prior to rifting, yet a narrow rift (<100 km wide at the surface) developed nonetheless. Dynamic models using finite element methods [e.g., *Dyksterhuis et al.*, 2007] show that narrow rifts can develop in a region with a weak lower crust if a single weakness is present in the inherited structure. A Neoproterozoic, Pan-African suture runs through Ethiopia, and on the basis of the step in crustal thickness across the CMER from the eastern to the western plateaus, *Keranen and Klemperer* [2008] interpreted the rift to follow the suture. *Stern* [2002] uses geochemical evidence to make the same argument, albeit with less ability to spatially constrain the suture. This Neoproterozoic suture likely provided the initial weakness necessary for narrow rifting to occur within the upper crust in the MER even with a weak lower crust that is deforming over a region >400 km wide including the entire northwestern Ethiopian Plateau.

[47] In the EARS further south in Kenya and Tanzania, the eastern and western branches have also formed as narrow rifts. These two branches wrap around the boundaries of the Tanzania craton [*Nyblade and Brazier*, 2002], and Pan-African suture thickening of the crust against the eastern margin of the Tanzania craton is suggested as a control on the location of the eastern branch [*Nyblade and Pollack*, 1992; *Tesha et al.*, 1997]. In Kenya and Tanzania the thermal structure of the region away from the Cenozoic rift is vastly different from the structure of the plateaus adjacent to the MER [*Julia et al.*, 2005; *Dugda*, 2007]. In contrast to the low-velocity lower crust away from the Cenozoic rift in Ethiopia, the lower crust in Tanzania has shear wave velocities between 3.9 and 4.1 km/s away from the Cenozoic rift [*Julia et al.*, 2005]. P wave tomography from the KRISP experiment [*Mechie et al.*, 1997] and the Kenya Broadband Seismic Experiment [*Park and Nyblade*, 2006] show a narrow, elongate low-velocity region beneath the rift itself, with normal seismic velocity (Vp > 8.0 km/s) beneath both rift shoulders. The lower crust and upper mantle in Kenya and Tanzania appears mafic, cool, and strong, with only the rift itself hot and weak.

[48] The northern and southern regions of the EARS have very different thermal profiles and vertical strength profiles (Figure 18 and Table 2), with an order-of-magnitude greater integrated lithospheric strength in the region adjacent to the eastern and western branches than in the plateaus adjacent to the Main Ethiopian Rift. Nonetheless, both systems have developed as classic examples of narrow, continental rifts. This similar development in diverse settings indicates that inherited structures, which were present in both cases as

the boundary of the craton to the south and as the suture to the north, were more important in controlling the mode of rifting than the rheological stratification. These inherited structures appear to be the primary control on the mode of continental rift development in East Africa.

Acknowledgments

[49] EAGLE data acquisition was funded by National Science Foundation (NSF) Continental Dynamics grant EAR0208475 and the Natural Environment Research Council. K. Keranen thanks the SEG Foundation and Anadarko for financial support during her Ph.D. We appreciate the continued willingness of Ethiopian scientists to host and collaborate with U.S. geophysicists. We thank Graham Stuart for sharing the EAGLE Phase I event data; EAGLE leadership for the coordination of the seismic project; the EBSE leaders for sharing their data; EAGLE and EBSE participants who helped with data collection; and Mulugeta Dugda, Tilahun Mammo, Ewenet Gashawbeza, Tyrone Rooney, Norm Sleep, Elizabeth Miller, and Chris Mattinson for valuable discussions. All five contributing authors of this manuscript significantly influenced and helped shape the final result. We appreciate very careful and constructive reviews from G. Corti and R. Bendick as well as helpful comments from the editor.

References

Abate, B., C. Koeberl, P. C. Buchanan, and W. Korner (1998), Petrography and geochemistry of basaltic and rhyodacitic rocks from Lake Tana and the Gimjabet-Kosober areas (North Central Ethiopia), *J. Afr. Earth Sci.*, *26*, 119–134, doi:10.1016/S0899-5362(97)00140-1.

Al-Mishwat, A. T., and S. J. Nasir (2004), Composition of the lower crust of the Arabian Plate: A xenolith perspective, *Lithos*, *72*, 45–72, doi:10.1016/j.lithos.2003.08.003.

Artemieva, I. M., and W. D. Mooney (2001), Thermal thickness and evolution of Precambrian lithosphere: A global study, *J. Geophys. Res.*, *106*, 16,387–16,414, doi:10.1029/2000JB900439.

Ayele, A., G. W. Stuart, and J.-M. Kendall (2004), Insights into rifting from SKS splitting and receiver functions: An example from Ethiopia, *Geophys. J. Int.*, *157*, 354–362, doi:10.1111/j.1365-246X.2004.02206.x.

Baker, J., L. Snee, and M. Menzies (1996), A brief Oligocene period of flood volcanism in Yemen, *Earth Planet. Sci. Lett.*, *138*, 39–55, doi:10.1016/0012-821X(95)00229-6.

Bastow, I. D., G. W. Stuart, J.-M. Kendall, and C. J. Ebinger (2005), Upper-mantle seismic structure in a region of incipient continental breakup: Northern Ethiopian rift, *Geophys. J. Int.*, *162*, 479–493, doi:10.1111/j.1365-246X.2005.02666.x.

Bastow, I. D., A. A. Nyblade, G. W. Stuart, T. O. Rooney, and M. H. Benoit (2008), Upper mantle seismic structure beneath the Ethiopian hot spot: Rifting at the edge of the African low-velocity anomaly, *Geochem. Geophys. Geosyst.*, *9*, Q12022, doi:10.1029/2008GC002107.

Bendick, R., S. McClusky, R. Bilham, L. Asfaw, and S. Klemperer (2006), Distributed Nubia-Somalia relative motion and dike intrusion in the Main Ethiopian Rift, *Geophys. J. Int.*, *165*, 303–310, doi:10.1111/j.1365-246X.2006.02904.x.

Benoit, M. H. (2005), The upper mantle seismic velocity structure beneath the Arabian Shield and East Africa, Ph.D. thesis, Pa. State Univ., University Park.

Benoit, M. H., A. A. Nyblade, and J. C. VanDecar (2006a), Upper mantle P wave speed variations beneath Ethiopia and the origin of the Afar hotspot, *Geology*, *34*, 329–332, doi:10.1130/G22281.1.

Benoit, M. H., A. A. Nyblade, and M. E. Pasyanos (2006b), Crustal thinning between the Ethiopian and East African Plateaus from modeling Rayleigh wave dispersion, *Geophys. Res. Lett.*, *33*, L13301, doi:10.1029/2006GL025687.

Berhe, S. M. (1990), Ophiolites in northeast and East Africa: Implications for Proterozoic crustal growth, *J. Geol. Soc.*, *147*, 41–57, doi:10.1144/gsjgs.147.1.0041.

Bonini, M., G. Corti, F. Innocenti, P. Manetti, F. Mazzarini, T. Abebe, and Z. Pecskay (2005), Evolution of the Main Ethiopian Rift in the frame of Afar and Kenya rifts propagation, *Tectonics*, *24*, TC1007, doi:10.1029/2004TC001680.

Brun, J.-P. (1999), Narrow rifts vs. wide rifts: Inferences for the mechanics of rifting from laboratory experiments, *Philos. Trans. R. Soc.*, *357*, 695–712, doi:10.1098/rsta.1999.0349.

Buck, W. R. (1991), Modes of continental lithospheric extension, *J. Geophys. Res.*, *96*, 20,161–20,178, doi:10.1029/91JB01485.

Burke, K., and A. M. C. Sengor (1986), Tectonic escape in the evolution of the continental crust, in *Reflection Seismology: The Continental Crust*, *Geodyn. Ser.*, vol. 14, edited by M. Barazangi and L. Brown, pp. 41–53, AGU, Washington, D. C.

Cammarano, F., S. Goes, P. Vacher, and D. Giardini (2003), Inferring upper-mantle temperatures from seismic velocities, *Phys. Earth Planet. Inter.*, *138*, 197–222, doi:10.1016/S0031-9201(03)00156-0.

Chang, S.-J., and C.-E. Baag (2005), Crustal structure in Southern Korea from joint analysis for teleseismic receiver functions and surface-wave dispersion, *Bull. Seismol. Soc. Am.*, *95*, 1516–1534, doi:10.1785/0120040080.

Chapman, D. S. (1986), Thermal gradients in the continental crust, in *The Nature of the Lower Continental Crust*, edited by J. B. Dawson et al., *Geol. Soc. Spec. Publ.*, *24*, 63–70.

Christensen, N. I. (1996), Poisson's ratio and crustal seismology, *J. Geophys. Res.*, *101*, 3139–3156, doi:10.1029/95JB03446.

Church, W. R. (1991), Discussion of "Ophiolites in northeast and East Africa: Implications for Proterozoic crustal growth,", *J. Geol. Soc.*, *48*, 600–606.

Conticelli, S., M. F. Sintoni, T. Abebe, F. Mazzarini, and P. Manetti (1999), Petrology and geochemistry of ultramafic xenoliths and host lavas from the Ethiopian Volcanic Province: An insight into the upper mantle under eastern Africa, *Acta Vulcanol.*, *11*, 143–159.

Corti, G. (2004), Centrifuge modelling of the influence of crustal fabrics on the development of transfer zones: Insights into the mechanics of continental rifting architecture, *Tectonophysics*, *384*, 191–208, doi:10.1016/j.tecto.2004.03.014.

Corti, G. (2008), Control of rift obliquity on the evolution and segmentation of the main Ethiopian rift, *Nat. Geosci.*, *1*, 258–262, doi:10.1038/ngeo160.

Dugda, M. (2007), Lithospheric structure beneath Eastern Africa from joint inversion of receiver functions and Rayleigh wave velocities, Ph.D. thesis, Pa. State Univ., University Park.

Dugda, M. T., A. A. Nyblade, J. Julia, C. A. Langston, C. J. Ammon, and S. Simiyu (2005), Crustal structure in Ethiopia and Kenya from receiver function analysis: Implications for

rift development in eastern Africa, *J. Geophys. Res.*, *110*, B01303, doi:10.1029/2004JB003065.

Dugda, M., A. A. Nyblade, and J. Julia (2007), Thin lithosphere beneath the Ethiopian Plateau revealed by a joint inversion of Rayleigh wave group velocities and receiver functions, *J. Geophys. Res.*, *112*, B08305, doi:10.1029/2006JB004918.

Dyksterhuis, S., P. Rey, R. D. Muller, and L. Moresi (2007), Effects of initial weakness on rift architecture, in *Imaging, Mapping and Modelling Continental Lithosphere Extension and Breakup*, edited by G. D. Karner, G. Manatschal, and L. M. Pinhiero, *Geol. Soc. Spec. Publ.*, *282*, 443–455.

Dziewonski, A. M., and D. L. Anderson (1981), Preliminary Reference Earth Model (PREM), *Phys. Earth Planet. Inter.*, *25*, 297–356, doi:10.1016/0031-9201(81)90046-7.

Faul, U. H., and I. Jackson (2005), The seismological signature of temperature and grain size variations in the upper mantle, *Earth Planet. Sci. Lett.*, *234*, 119–134, doi:10.1016/j.epsl.2005.02.008.

Faul, U. H., D. R. Toomey, and H. S. Waff (1994), Intergranular basaltic melt is distributed in thin, elongated inclusions, *Geophys. Res. Lett.*, *21*, 29–32, doi:10.1029/93GL03051.

Foster, A., C. Ebinger, E. Mbede, and D. Rex (1997), Tectonic development of the northern Tanzanian sector of the East African Rift System, *J. Geol. Soc.*, *154*, 689–700, doi:10.1144/gsjgs.154.4.0689.

Gashawbeza, E. M., S. L. Klemperer, A. A. Nyblade, K. T. Walker, and K. M. Keranen (2004), Shear-wave splitting in Ethiopia: Precambrian mantle anisotropy locally modified by Neogene rifting, *Geophys. Res. Lett.*, *31*, L18602, doi:10.1029/2004GL020471.

Gok, R., H. Mahdi, H. Al-Shukri, and A. Rodgers (2008), Crustal structure of Iraq from receiver functions and surface wave dispersion: Implications for understanding the deformation history of the Arabian-Eurasian collision, *Geophys. J. Int.*, *172*, 1179–1187, doi:10.1111/j.1365-246X.2007.03670.x.

Hashin, Z., and A. Shtrikman (1962), A variational approach to the theory of effective magnetic permeability of multiphase materials, *J. Appl. Phys.*, *33*, 3125–3131, doi:10.1063/1.1728579.

Hermance, J. F. (1979), The electrical conductivity of materials containing partial melt: A simple model from Archie's Law, *Geophys. Res. Lett.*, *6*, 613–616, doi:10.1029/GL006i007p00613.

Hirschmann, M. M., M. S. Ghiorso, L. E. Wasylenki, P. D. Asimow, and E. M. Stolper (1998), Calculation of peridotite partial melting from thermodynamic models of minerals and melts. I. Review of methods and comparison with experiments, *J. Petrol.*, *39*, 1091–1115, doi:10.1093/petrology/39.6.1091.

Hirth, G., and D. Kohlstedt (2003), Rheology of the upper mantle and the mantle wedge: A view from experimentalists, in *Inside the Subduction Factory*, *Geophys. Monogr. Ser.*, vol. 138, edited by J. Eiler, pp. 83–105, AGU, Washington, D. C.

Hofmann, C., V. Courtillot, G. Feraud, P. Rochette, G. Yirgu, E. Ketefo, and R. Pik (1997), Timing of the Ethiopian flood basalt event: Implications for plume birth and global change, *Nature*, *389*, 838–841, doi:10.1038/39853.

Horspool, N. A., M. K. Savage, and S. Bannister (2006), Implications for intraplate volcanism and back-arc deformation in northwestern New Zealand, from joint inversion of receiver functions and surface waves, *Geophys. J. Int.*, *166*, 1466–1483, doi:10.1111/j.1365-246X.2006.03016.x.

Julia, J. (2007), Constraining velocity and density contrasts across the crust–mantle boundary with receiver function amplitudes, *Geophys. J. Int.*, *171*, 286–301, doi:10.1111/j.1365-2966.2007.03502.x.

Julia, J., C. J. Ammon, R. B. Herrmann, and A. M. Correig (2000), Joint inversion of receiver functions and surface wave dispersion observations, *Geophys. J. Int.*, *143*, 99–112, doi:10.1046/j.1365-246x.2000.00217.x.

Julia, J., C. J. Ammon, and R. B. Herrmann (2003), Lithospheric structure of the Arabian Shield from the joint inversion of receiver functions and surface-wave group velocities, *Tectonophysics*, *371*, 1–21, doi:10.1016/S0040-1951(03)00196-3.

Julia, J., C. J. Ammon, and A. A. Nyblade (2005), Evidence for mafic lower crust in Tanzania, East Africa, from joint inversion of receiver functions and Rayleigh wave dispersion velocities, *Geophys. J. Int.*, *162*, 555–569, doi:10.1111/j.1365-246X.2005.02685.x.

Kampfmann, W., and H. Berckhemer (1985), High temperature experiments on the elastic and anelastic behaviour of magmatic rocks, *Phys. Earth Planet. Inter.*, *40*, 223–247, doi:10.1016/0031-9201(85)90132-3.

Keir, D., J.-M. Kendall, and C. Ebinger (2005), Variations in late syn-rift melt alignment inferred from shear-wave splitting in crustal earthquakes beneath the Ethiopian rift, *Geophys. Res. Lett.*, *32*, L23308, doi:10.1029/2005GL024150.

Kendall, J.-M., G. Stuart, C. Ebinger, I. Bastow, and D. Keir (2005), Magma assisted rifting in Ethiopia, *Nature*, *433*, 146–148, doi:10.1038/nature03161.

Keranen, K., and S. L. Klemperer (2008), Discontinuous and diachronous evolution of the Main Ethiopian Rift: Implications for the development of continental rifts, *Earth Planet. Sci. Lett.*, *265*, 96–111, doi:10.1016/j.epsl.2007.09.038.

Keranen, K., S. L. Klemperer, R. Gloaguen, and the EAGLE Working Group (2004), Three-dimensional seismic imaging of a protoridge axis in the Main Ethiopian rift, *Geology*, *32*, 949–952, doi:10.1130/G20737.1.

Kern, H., T. Popp, F. Gorbatsevich, A. Zharikov, K. V. Lobanov, and Y. P. Smirnov (2001), Pressure and temperature dependence of VP and VS in rocks from the superdeep well and from surface analogues at Kola and the nature of velocity anisotropy, *Tectonophysics*, *338*, 113–134, doi:10.1016/S0040-1951(01)00128-7.

Kieffer, B., et al. (2004), Flood and shield basalts from Ethiopia: Magmas from the African Superswell, *J. Petrol.*, *45*, 793–834, doi:10.1093/petrology/egg112.

Larson, E. W. F., and G. Ekström (2001), Global models of surface wave group velocity, *Pure Appl. Geophys.*, *158*, 1377–1400, doi:10.1007/PL00001226.

Lawrence, J. F., and D. A. Wiens (2004), Combined receiver-function and surface wave phase-velocity inversion using a niching genetic algorithm: Application to Patagonia, *Bull. Seismol. Soc. Am.*, *94*, 977–987, doi:10.1785/0120030172.

Ligorria, J. P., and C. Ammon (1999), Iterative deconvolution and receiver-function estimation, *Bull. Seismol. Soc. Am.*, *89*, 1395–1400.

Macdonald, R. (2002), Magmatism of the Kenya Rift Valley: A review, *Trans. R. Soc. Edinburgh Earth Sci.*, *93*, 239–253.

Mackenzie, G. D., H. Thybo, and P. K. H. Maguire (2005), Crustal velocity structure across the main Ethiopian Rift: Results from two-dimensional wide-angle seismic modelling, *Geophys. J. Int.*, *162*, 994–1006, doi:10.1111/j.1365-246X.2005.02710.x.

Maguire, P. K. H., et al. (2003), Geophysical project in Ethiopia studies continental breakup, *Eos Trans. AGU*, *84*, 342–343, doi:10.1029/2003EO350002.

Maguire, P. K. H., et al. (2006), Crustal structure of the northern Main Ethiopian Rift from the EAGLE controlled-source survey; a snapshot of incipient lithospheric break-up, in *The Afar Volcanic Province Within the East African Rift System*, edited by G. Yirgu, C. J. Ebinger, and P. K. H. Maguire, *Geol. Soc. Spec. Publ.*, *259*, 269–292.

Manatschal, G., O. Müntener, L. L. Lavier, T. A. Minshull, and G. Péron-Pinvidic (2007), Observations from the Alpine Tethys and Iberia–Newfoundland margins pertinent to the interpretation of continental breakup, in *Imaging, Mapping and Modelling Continental Lithosphere Extension and Breakup*, edited by G. D. Karner, G. Manatschal, and L. M. Pinhiero, *Geol. Soc. Spec. Publ.*, *282*, 291–324.

Mansur, A. T., S. Manya, and R. L. Rudnick (2006), Composition and thermal history of the lower crust beneath the Tanzania Craton and the adjacent Mozambique Belt, *Eos Trans. AGU*, *87*(36), Jt. Assem. Suppl., Abstract S23A-06.

McGuire, A. V., and R. J. Stern (1993), Granulite xenoliths from western Saudi Arabia; the lower crust of the late Precambrian Arabian–Nubian Shield, *Contrib. Mineral. Petrol.*, *114*, 395–408, doi:10.1007/BF01046541.

Mechie, J., C. Prodehl, G. R. Keller, M. A. Khan, and S. J. Gaciri (1997), A model for structure, composition and evolution of the Kenya rift, in *Structure and Dynamic Processes in the Lithosphere of the Afro-Arabian Rift System*, edited by K. Fuchs et al., *Tectonophysics*, *278*, 95–119.

Meert, J. G., and B. S. Lieberman (2008), The Neoproterozoic assembly of Gondwana and its relationship to the Ediacaran-Cambrian radiation, *Gondwana Res.*, *14*, 5–21, doi:10.1016/j.gr.2007.06.007.

Menke, W., M. West, B. Brandsdottir, and D. Sparks (1998), Compressional and shear velocity structure of the lithosphere in northern Iceland, *Bull. Seismol. Soc. Am.*, *88*, 1561–1571.

Merzer, A. M., and S. L. Klemperer (1992), High electrical conductivity in a model lower crust with unconnected, conductive, seismically reflective layers, *Geophys. J. Int.*, *108*, 895–905, doi:10.1111/j.1365-246X.1992.tb03478.x.

Mohr, P. (1983), Ethiopian flood basalt province, *Nature*, *303*, 577–584, doi:10.1038/303577a0.

Nyblade, A. A., and R. Brazier (2002), Precambrian lithospheric controls on the development of the East African rift system, *Geology*, *30*, 755–758, doi:10.1130/0091-7613(2002)030<0755:PLCOTD>2.0.CO;2.

Nyblade, A. A., and C. A. Langston (2002), Broadband seismic experiments probe the East African rift, *Eos Trans. AGU*, *83*, 405–408, doi:10.1029/2002EO000296.

Nyblade, A. A., and H. N. Pollack (1992), A gravity model for the lithosphere in western Kenya and northeastern Tanzania, *Tectonophysics*, *212*, 257–267, doi:10.1016/0040-1951(92)90294-G.

Nyblade, A. A., H. N. Pollack, D. L. Jones, F. Podmore, and M. Mushayandebvu (1990), Terrestrial heat flow in east and southern Africa, *J. Geophys. Res.*, *95*, 17,371–17,384, doi:10.1029/JB095iB11p17371.

Park, Y., and A. A. Nyblade (2006), P wave tomography reveals a westward dipping low velocity zone beneath the Kenya Rift, *Geophys. Res. Lett.*, *33*, L07311, doi:10.1029/2005GL025605.

Pasyanos, M. E. (2005), A variable resolution surface wave dispersion study of Eurasia, North Africa, and surrounding regions, *J. Geophys. Res.*, *110*, B12301, doi:10.1029/2005JB003749.

Pasyanos, M. E., W. R. Walter, and S. E. Hazler (2001), A surface wave dispersion study of the Middle East and North Africa for monitoring the Comprehensive Nuclear-Test-Ban Treaty, *Pure Appl. Geophys.*, *158*, 1445–1474, doi:10.1007/PL00001229.

Priestley, K., and D. McKenzie (2006), The thermal structure of the lithosphere from shear wave velocities, *Earth Planet. Sci. Lett.*, *244*, 285–301, doi:10.1016/j.epsl.2006.01.008.

Ranalli, G. (1997), Rheology of the lithosphere in space and time, *Geol. Soc. Spec. Publ.*, *121*, 19–37, doi:10.1144/GSL.SP.1997.121.01.02.

Roberts, J. J., and J. A. Tyburczy (1999), Partial-melt electrical conductivity: Influence of melt composition, *J. Geophys. Res.*, *104*, 7055–7065, doi:10.1029/1998JB900111.

Schilling, F. R., et al. (2006), Partial melting in the central Andean crust: A review of geophysical, petrophysical, and petrologic evidence, in *The Andes: Active Subduction Orogeny*, part IV, edited by O. Oncken et al., pp. 459–474, Springer, Berlin.

Shackleton, R. M. (1986), Precambrian collision tectonics in Africa, in *Collision Tectonics*, edited by M. P. Coward and A. C. Reis, *Geol. Soc. Spec. Publ.*, *19*, 329–349.

Sokoutis, D., G. Corti, M. Bonini, J. P. Brun, S. Cloetingh, T. Mauduit, and P. Manetti (2007), Modelling the extension of heterogeneous hot lithosphere, *Tectonophysics*, *444*, 63–79, doi:10.1016/j.tecto.2007.08.012.

Stern, R. J. (1994), Arc assembly and continental collision in the Neoproterozoic East African orogen, *Annu. Rev. Earth Planet. Sci.*, *22*, 319–351.

Stern, R. J. (2002), Crustal evolution in the East African Orogen: A neodymium isotopic perspective, *J. Afr. Earth Sci.*, *34*, 109–117, doi:10.1016/S0899-5362(02)00012-X.

Stern, R. J., K. C. Nielsen, E. Best, M. Sultan, R. E. Arvidson, and A. Kroner (1990), Orientation of the late Precambrian sutures in the Arabian-Nubian Shield, *Geology*, *18*, 1103–1106, doi:10.1130/0091-7613(1990)018<1103:OOLPSI>2.3.CO;2.

Stuart, G. W., I. D. Bastow, and C. J. Ebinger (2006), Crustal structure of the northern Main Ethiopian Rift from receiver function studies, in *The Afar Volcanic Province Within the East African Rift System*, edited by G. Yirgu, C. J. Ebinger, and P. K. H. Maguire, *Geol. Soc. Spec. Publ.*, *259*, 253–267.

Tesha, A. L., A. A. Nyblade, G. R. Keller, and D. I. Doser (1997), Rift localization in suture-thickened crust: Evidence from Bouguer gravity anomalies in northeastern Tanzania, *Tectonophysics*, *278*, 315–328, doi:10.1016/S0040-1951(97)00110-8.

Tkalcic, H., M. Pasyanos, A. Rodgers, R. Gok, W. Walter, and A. Al-Amri (2006), A multi-step approach in joint modeling of surface wave dispersion and teleseismic receiver functions: Implications for lithospheric structure of the Arabian peninsula, *J. Geophys. Res.*, *111*, B11311, doi:10.1029/2005JB004130.

Ukstins, I., P. Renne, E. Wolfenden, J. Baker, and M. Menzies (2002), Matching conjugate volcanic rifted margins: $^{40}Ar/^{39}Ar$ chrono-stratigraphy of pre- and syn-rift bimodal flood volcanism in Ethiopia and Yemen, *Earth Planet. Sci. Lett.*, *198*, 289–306, doi:10.1016/S0012-821X(02)00525-3.

Vail, J. R. (1985), Pan-African (late Precambrian) tectonic terrains and the reconstruction of the Arabian-Nubian Shield, *Geology*, *13*, 839–849, doi:10.1130/0091-7613(1985)13<839:PLPTTA>2.0.CO;2.

van Wijk, J. W. (2005), Role of weak zone orientation in continental lithosphere extension, *Geophys. Res. Lett.*, *32*, L02303, doi:10.1029/2004GL022192.

Whaler, K. A., and S. Hautot (2006), The electrical resistivity structure of the crust beneath the northern Main Ethiopian Rift, in *The Afar Volcanic Province Within the East African Rift System*, edited by G. Yirgu, C. J. Ebinger, and P. K. H. Maguire, *Geol. Soc. Spec. Publ.*, *259*, 293–305.

Zhu, L., and H. Kanamori (2000), Moho depth variation in southern California from teleseismic receiver functions, *J. Geophys. Res.*, *105*, 2969–2980, doi:10.1029/1999JB900322.